# An overview on nitride and nitrogen-doped photocatalysts for energy and environmental applications

Wenjun Wang [a, b,1], Ming Chen [a, b,1], Danlian Huang [a, b,1], Guangming Zeng [a, b, *], Chen Zhang [a, b, *], Cui Lai [a, b], Chengyun Zhou [a, b], Yang Yang [a, b], Min Cheng [a, b], Liang Hu [c, d], Weiping Xiong [a, b], Zhihao Li [a, b]; Ziwei Wang [a, b]

*a College of Environmental Science and Engineering, Hunan University, Changsha, 410082, P.R. China*

*b Key Laboratory of Environmental Biology and Pollution Control, Ministry of Education, Hunan University, Changsha 410082, P.R. China*

*c School of Minerals Processing and Bioengineering, Central South University, Changsha, 410083, P.R. China*

*d Key Laboratory of Biohydrometallurgy, Ministry of Education, Central South University, Changsha, 410083, P.R. China*

Accepted MS

[*] Corresponding authors at: College of Environmental Science and Engineering, Hunan University, Changsha 410082, PR China.

*E-mail addresses*: zgming@hnu.edu.cn (G. Zeng), zhangchen@hnu.edu.cn (C. Zhang).

[1] These authors contribute equally to this article.

**Abstract**

Semiconductor-based photocatalysis can utilize solar energy to solve the problems of energy crisis and environmental pollution. How to construct a visible-light-driven (VLD) photocatalyst was the key to efficient use of solar energy. In recent decades, nitrogen (N) resources have attained increasing interest benefit from its outstanding properties and abundant reserves. In addition, nitride and nitrogen-doped (N-doped) photocatalysts have attracted much attention owing to their unique structures, excellent physicochemical stability and low-cost. However, few reviews focus on the nitride and N-doped photocatalysts with high photocatalytic activity. Herein, the critical review summarized the recent progresses and advances in the preparation, properties and applications of nitride and N-doped photocatalysts in hydrogen evolution from water, environmental pollutants removal, carbon dioxide reduction etc. Meanwhile, the current challenges and prospects were also presented. This review aims to summarized the recent researches on nitride and N-doped photocatalysts for environmental applications and energy-related, and provide a constructive guidelines for this booming research topic.

**Keywords**

Photocatalysis; Nitride nanomaterials; Energy generation; Environmental purification; Carbon nitride

Accepted MS

## 1. Introduction

In our modern society, fossil fuels are the world's main sources of energy. However, they are limited and non-renewable resources in nature [1-12]. Overexploitation of fossil fuels leads to energy crisis that threatens national security [13-20]. In addition, the consumption of fossil fuels produces large amounts of gases (greenhouse gases and toxic gases) and causes environmental pollution [21-27]. Therefore, green and sustainable alternatives are highly desired for the development of our modern society [28-33]. Compared to the traditional method, photocatalytic technology shows superior performance and has been widely investigated in energy generation and pollutant treatment solving in recent years [34-39].

According to previous literature, choosing an appropriate photocatalyst was crucial for whole reaction, because different photocatalysts with various properties can lead to different experimental results [40]. In the past decades, various photocatalysts such as CdS [41], $TiO_2$ [42], ZnO [43], $SnO_2$ [44], $WO_3$ [45], BN-based [46], and g-$C_3N_4$ [40] have been studied. Among them, metal-free g-$C_3N_4$ becomes a rising "star" materials in photocatalysis field owing to its unique two-dimensional structure, high stability and visible light response. Furthermore, g-$C_3N_4$ is earth-abundant and easily obtained via one-step polymerization of cheap raw material like cyanamide [47], dicyandiamide [48], urea [40], melamine [49], and thiourea [50]. In addition, "white graphene"—hexagonal boron nitride (h-BN) is another "hot" nanomaterial due to the graphene analogue layered structure. Moreover, compared with graphene, boron nitride (BN) shows better physical, chemical and

Accepted MS

optical properties [51, 52]. Metal oxide nanostructures, such as $SnO_2$, ZnO, $TiO_2$ ZnO, and $Fe_2O_3$, have attracted considerable research interest because of their great potential in the photocatalytic oxidation of organic pollutants [53-57]. Among the metal oxide nanostructures, $TiO_2$ is one of the most classic photocatalyst, which has been mostly investigated in the fields of energy generation and pollutant treatment because of its relatively high photocatalytic activity, nontoxicity, and low production costs [58]. Nevertheless, the usage rate of $TiO_2$ in photocatalysis field is not very high on account of its wide band gap [59, 60]. Hence, the ways of tuning band gap of $TiO_2$ will have a positive effect on its practical applications. Element doping is identified as an efficient method to tune band gap of $TiO_2$, shift optical response of $TiO_2$ and can enhance the charge separation. $TiO_2$ doped with metal element (K, Pd, Fe, W, Zr and Cu) and various non-metal elements (N, F, S, B, C and P) have been carried out for improving its photocatalytic activities [58]. Among them, nitrogen doped $TiO_2$ shows better performance and is taken for the most promising investigation since N and O present similar structural, chemical and electronic features (electronegativity, polarizability, ionic radii and coordination numbers) [61-64]. Nitrogen doped $TiO_2$ exhibits broad absorption in the visible region, which could allow the utilization of a large part of the solar spectrum [65, 66]. This might be helpful for energy and environmental applications, such as water splitting, carbon dioxide reduction, and degradation of pollutions.

It was worth noting that g-$C_3N_4$, BN, N-$TiO_2$ and other N-dopant have constituted a series of sustainable, environment benign, low-cost, and earth-abundant

Accepted MS

semiconductor for applications in hydrogen evolution from water, the degradation of contaminants and carbon dioxide reduction. There were many excellent reviews about $TiO_2$ and g-$C_3N_4$ photocatalyst [58, 67-69], but rare reviews were about BN and N-$TiO_2$. Furthermore, very few reviews were focused on nitride and N-doped photocatalysts and their application in the past few years. Many reviews can also be found mainly focusing on synthesis and catalytic applications of carbon-based nanomaterials [70-76]. However, the nitride photocatalysts were scarcely described in the literature, and their economic potential and photocatalytic performance was completely overlooked [77]. Therefore, the paper, aiming to summarize the preparation, properties, and applications in energy and environmental issues of nitride and N-doped photocatalyst was necessary. Herein, we introduced a renewed review which summarizes the synthesis methods, properties, and applications of nitride and N-doped photocatalysts. Firstly, the preparation methods of nitride photocatalysts were discussed. Secondly, the structure and properties of nitride photocatalysts were presented. Furthermore, recent progresses on water splitting, carbon dioxide reduction, degradation of pollutions of nitride and N-doped photocatalysts were reviewed. Finally, the existing challenges and future outlooks were also summarized and discussed.

Accepted MS

## 2. Synthesis methods

### 2.1 Synthesis of g-$C_3N_4$

Graphite carbon nitride, as an analog of graphite, has become a hot material for

environmental remediation due to its unique structure and potential application prospects [68, 78]. In the past decades, people have tried various ways to synthesize g-$C_3N_4$ materials including solvothermal method [79-82], solid-state reaction [83-85], thermal polymerization [86] and electrochemistry deposition method [87, 88]. The synthesis methods of g-$C_3N_4$ were illustrated in Table 1, and including the advantages and disadvantages.

### 2.1.1 Solvothermal method

The solvothermal method was used to synthesize various functional materials due to the advantages of the uniformity of the reaction system, less pollution and mild reaction conditions [79]. Wang and coworkers successfully synthesized g-$C_3N_4$ by using melamine and cyanuric chloride as precursor with acetonitrile, benzene, chloroform as solvent, respectively [80]. When the reaction temperature reached 180 $^{o}$C in acetonitrile, a diameter of about 50 nm and 10 nm in length of uniformly g-$C_3N_4$ nanorods were prepared and shown in Fig. 1a-b. Furthermore, the classic polymerization route was exemplified in Fig. 1c. Solvothermal method can control temperature to prepare special structure of g-$C_3N_4$. Cao and his co-works used a simple solvothermal method to prepare a series of one-dimensional (1D) g-$C_3N_4$: aligned nanoribbons and nanotube bundles by changing the reaction condition including the pressure, temperature and reaction time [81, 82]. The method has the disadvantages that the reaction conditions are difficult to control and the industrial production is difficult to realize in the process of preparing g-$C_3N_4$.

### 2.1.2 Solid-state reaction

Accepted MS

Solid-state reaction was an ideal method to prepare g-$C_3N_4$ since it can control the morphology of g-$C_3N_4$. Various morphologies including nanospheres [89], nanowires [90], nanotubes [83], hollow spheres [84] and nanofibers [85] of g-$C_3N_4$ have been obtained. Khabashesku et al. used $Li_3N$ as a nitrogen-bridging agent and fluoride or cyanuric chloride as an s-triazine precursor to prepare a hollow spherical unshaped g-$C_3N_4$ by optimizing temperature pressure and other reaction conditions [84]. Furthermore, Li et al. used melamine instead of $Li_3N$ to prepare carbon nitride hollow vessels [83].

**2.1.3 Thermal polymerization**

Thermal polymerization is the most popular strategy for the preparation of g-$C_3N_4$ due to its simple operation, short preparation cycle and large productivity [86]. The product of thermal polymerization prepared g-$C_3N_4$ including carbon rich (C/N molar ratio range is 1 ~ 5) g-$C_3N_4$ with poor crystallinity and nitrogen rich (C/N molar ratio range is 0.6 ~ 1) g-$C_3N_4$ with good crystallinity [91, 92]. For example, Zhang and coworkers reported thermal condensation method that entails using acetic-treated melamine as a precursor to synthesize nitrogen deficient g-$C_3N_4$, which acted as a photocatalyst for generation of hydrogen through water splitting and photocatalytic degradation of Rhodamine B (RhB) [93]. In Zhao's works, g-$C_3N_4$ polymer was successfully prepared via a fractional thermal polymerization process and g-$C_3N_4$ obtained from different temperature and raw materials: melamine, guanidine carbonate and dicyandiamide [94].

Thermal polymerization preparation process of g-$C_3N_4$ is fairly unstable,

Accepted MS

different degrees of polycondensation reaction can coexist in a wide temperature range, so it is difficult to prepare a single molecular structure of carbon nitride materials [40]. Furthermore, materials are prone to decompose mildly at 600 $^{o}$C, while decompose sharply at 700 $^{o}$C, and then generated gas such as $NH_3$ and $C_xN_yH_z$ which are harm to human. The best annealing temperature of synthesized g-$C_3N_4$ nanosheets in Ar atmosphere was 550 ℃ [40].

### 2.1.4 Electrochemistry deposition method

Electrochemical deposition is widely used in the preparation of many solid materials due to its simple equipment, easy control and no need for high temperature and high pressure. This method has been used for preparation of g-$C_3N_4$ films in recent years since it can reduce the reaction temperature of the nitride carbon generating system and the reaction potential of C and N atoms bonding [87, 88]. Cao et al. successfully prepared the g-$C_3N_4$ thin film on Si substrate by electrodeposition method [87, 88]. Electrochemical deposition method can also be combined with template method for the purpose of adjusting the morphology of carbon nitride. For example, Cao's group used a simple electrodeposition method to prepared hollow g-$C_3N_4$ microspheres with exist of silica nanospheres template. And the size of obtained g-$C_3N_4$ microspheres was 5–30 nm, which was obviously different from the previous turbostraticor or graphite-like g-$C_3N_4$ sphere with smooth wall microstructures [89].

## 2.2 Synthesis of BN

Hexagonal boron nitride was also named "white graphene" since its layered

Accepted MS

structure is similar to graphene, whose layer is composed of B and N atoms arranged alternately unlimited extension of hexagonal honeycomb structure [95, 96]. The structure of hexagonal boron nitride (h-BN) was depicted in Fig. 2. However, boron nitride (BN) has better physical, chemical and optical properties than graphene [51, 52]. There were a lot of methods to prepare h-BN nanomaterials including chemical exfoliation, mechanical exfoliation, chemical vapor deposition (CVD), ultrasonic-assisted liquid phase exfoliation and other methods. These methods have been refined in Table 2.

**2.2.1 Mechanical exfoliation**

Mechanical exfoliation can generate nanosheets with perfect crystalline. Therefore many researchers have applied the mechanical exfoliation method to explore the intrinsic properties of the nanomaterials with wonderful sheets [95]. The mechanical exfoliation method was primarily applied to separate graphene monolayers by Novoselov. Since then, multiplicity layered BN was successfully prepared by this method [96, 97]. However, compared to prepared graphene, this technique was difficult to render a certain yield of few-layered and monolayered BN. Pacile et al. obtained thin sheets of h-BN and established their crystallinity by the micromechanical cleavage technique. The key step of peeling off few-layered h-BN was attached BN power to a 300 nm thick $SiO_2$ substrate with adhesive tape, and then forced to separate it [98].

Another pattern of mechanical exfoliation was ball milling method via the utilization of shear forces to isolate BN nanosheets [99, 100]. For example, Li et al.

Accepted MS

obtained high quality and high yield BN nanosheets by ball milling method. Fig. 3a and Fig. 3c illustrates two intermediate stages in h-BN preparation process. The laminated thin h-BN nanosheets were caused by milling ball colliding, exfoliation mechanisms and models of this process were also shown in Fig. 3. In this process, benzyl benzoate was used for decreasing milling contamination and ball impacts [99]. Moreover, in the interaction of Lewis acid−base between boron atoms and amino groups, Lin et al. prepared layered h-BN nanosheets with long hydrophilic or lipophilic chains [100].

**2.2.2 Chemical vapor deposition**

CVD was a technique for forming solid deposits at the gas-solid interface using a gaseous or vapor state, which was capable of synthesizing graphene and h-BN layers on a large scale [52, 101, 102]. Laurie and colleagues prepared BN nanotubes by CVD method at temperatures around 1100 ℃. In this process, borazine ($B_3N_3H_6$) was used as a precursor and Co, Ni, NiB, $Ni_2B$ were particulate catalysts [103]. Gao et al. successfully synthesized a controllable thickness (25-50 nm) of h-BN nanosheets via catalyst-free CVD process under the condition of 1100-1300 $^{o}$C [104]. Many researchers synthesize h-BN thin films by CVD method with different precursors. Commixture nitrogen and boron precursors such as $NH_3/BCl_3$[105], $NH_3/B_2H_6$ [106], and $NH_3/BF_3$[107] were employed to prepared h-BN nanosheets. In above systems, control of boron source and the gas flow rate was vital for preparing h-BN layers. In addition, the deposition rate was affected by the mole ratio of boron source and $NH_3$. Furthermore, there were a lot of researches about the single boron source like

Accepted MS

borazine ($B_3N_3H_6$), hexachloroborazine ($B_3N_3Cl_6$), and trichloroborazine ($B_3N_3H_3Cl_3$) attain BN nanosheets [108-110]. For example, Shi et al. use $B_3N_3H_6$ as the precursor material to prepare smooth surface BN thin film by CVD method. In the process, the growth temperature can be decreased to 400 $^{o}$C [111]. Compared to the mechanical exfoliation method, CVD method cannot easily manipulate the layer number and produce high yield of h-BN nanosheets. Therefore, the dry CVD method has been explored and was used for the synthesis of several layered BN nanomaterials on a large scale and high yield [95, 103].

**2.2.3 Chemical exfoliation**

The chemical stripping method reacts in solution, and the free movement of the reaction product can conquer the van der Waals force to obtain BN nanosheets [51]. Han et al. firstly prepared few-layer and mono-layer h-BN nanosheets via chemical-solution-derived method in 2008 [51, 112]. In this process, 0.2 mg of BN crystal was sonicated in a 5 mL of 1,2-dichloroethane solution for 1 h to decompose h-BN crystal into several layers of h-BN nanosheets [112]. Among the methods of prepared single- and few-layered h-BN nanosheets, wet chemical reaction was one of meaning methods. Nag et al. synthesized about 1-4 layers of BN nanosheets by reacting different proportions of urea and boric acid under high temperature in $N_2$ atmosphere. Interestingly, the final BN nanosheets exhibit negligible $H_2$ adsorption but exhibit high $CO_2$ adsorption [113]. Although the chemical stripping method has many advantages, the yield of the product obtained by this method was not high.

**2.2.4 Ultrasonic-assisted liquid phase exfoliation**

Accepted MS

Ultrasound-assisted liquid phase exfoliation produces dispersed two-dimensional BN nanomaterials in different aqueous or solvent surfactant solutions [95]. Lin and colleagues have shown that water can effectively remove the layered h-BN structure to form a "clean" aqueous dispersion of h-BN nanosheets with the help of sonication [114]. Under ultrasonic conditions, the shedding mechanism was BN hydrolysis, and the adjacent borazine units were hydrolyzed to the edges, the defects were further diffused. The final result was "cutting" the large h-BN sheets into a single layer and several layers of nanosheets and reducing the lateral dimension in water dispersion [114]. These progress and exfoliation mechanisms are shown in Fig. 4. Compared with mechanical exfoliation and other methods, liquid-phase exfoliation is an efficient method to obtained large quantities of single-layer and multi-layer materials. But it should be known that the controlling of the lateral size and the number of layers was difficult [95, 115].

Accepted MS

## 3. Properties of nitride photocatalysis

The nitride and N-doped materials possess wide physicochemical properties especially in pollutant treatment and energy generation. The typical nitride materials including g-$C_3N_4$, BN, N-$TiO_2$ and so on, which have the ability to generate energy and degrade pollutants [116, 117]. The nitrogen economy is a proposed future system in which nitride compounds are produced to help meet the demands of energy sectors and environment protection agency [77].

### 3.1 g-$C_3N_4$

There are five structures (graphite phase, quasi cubic phase, cubic phase, beta phase and alpha phase) of carbon nitride, and graphite phase is just one of them [118]. As a graphite analogue, g-$C_3N_4$ also has nanosheet structure including $C_3N_3$ rings and $C_6N_7$ rings. With the characteristic band-gap structure and highly conjugated electron pair of N atom, g-$C_3N_4$ has been become the "rising star" semiconductor material [49, 69]. Moreover, g-$C_3N_4$ has stable physicochemical properties, low-cost and large specific surface area, it also can be easily fabricated from available precursors like melamine, urea, cyanamide, dicyandiamide and etc [68]. A fundamental understanding of these chemical and structural properties will guide us build g-$C_3N_4$-based photocatalysts with high photocatalytic performance.

### 3.1.1 Stability properties

The stability of a material includes thermal and chemical stability. As an organic substance, carbon nitride can be heat-resistant to 550-600 $^{o}$C in air. For instance, Zhang et al. used pyrolytic thiourea method to prepared g-$C_3N_4$, and the g-$C_3N_4$ starts to decompose rapidly at 550 $^{o}$C [119]. Furthermore, the thermal stability of g-$C_3N_4$ synthesized by different preparation methods is slightly different, which is probably related to different degrees of condensation of the starting compounds. The complete decomposition temperature of g-$C_3N_4$ occurs at about 750 $^{o}$C [120]. It should be noted that the thermal stability of g-$C_3N_4$ has been regarded to be the highest among organic materials [121-124]. In addition, the g-$C_3N_4$ also reveals excellent chemical stability. The g-$C_3N_4$ is not dissolved in the most part of solvents such as acid, alkali, water, and various organic solvents (toluene, ethanol, diethyl, etc) because of its interlayer

Accepted MS

van der Waals force. Interestingly, the protonation effects and wonderful acid stability of g-$C_3N_4$ has further confirmed by Zhu and coworkers [125].

### 3.1.2 Optical and electronic properties

Graphite carbon nitride has good optical and electronic properties, and the typical ultraviolet–visible absorption spectrum of g-$C_3N_4$ synthesized at different temperature were depicted in Fig. 5a [126, 127]. It can be noted that these two samples fabricated at 550 and 600 $^{o}$C show similar bandgap absorption edges (about 450nm). In particular, the bandgap of g-$C_3N_4$ synthesized at 550 $^{o}$C is estimated to be 2.7 eV, which is consistent with previous results [128-130]. As depicted in the inset of Fig. 5a, the color of g-$C_3N_4$ powder is greyish yellow, which further verified the favorable medium band gap for vis absorption. Apart from the optical properties, suitable electronic properties also play crucial roles in photocatalysis. The electronic properties and charge carrier dynamics (carriers generation, recombination, separation, and transfer) are studied by many different advanced techniques, such as photoluminescence (PL), Nyquist impedance plots, transient photocurrent decay, photocurrent response and surface photovoltaic technique (SPV), etc [131-137]. For example, Xie et al. used the SPV and PL technology to test the separation efficiency of lightgenerated carriers of g-$C_3N_4$-based photocatalysts [138]. From Fig. 5b, the photovoltage response region of bare g-$C_3N_4$ (Ni0) and g-$C_3N_4$ loaded Ni (Ni10) is in the range of 300–450 nm. The photoelectric signal of Ni10 is stronger than Ni0, suggesting Ni10 obtained a higher carriers separation efficiency. As a co-catalyst, Ni nanoparticles can effectively promote charge separation efficiency of g-$C_3N_4$. With

Accepted MS

the constant efforts of the researchers, many other properties (adsorption, crystal structural, surface physicochemical, photoelectrochemical, and electrochemical) of carbon nitride have been continuously discovered [139, 140].

### 3.2 BN

Rhombohedral BN (r-BN), hexagonal BN (h-BN), wurtzite BN (w-BN) and diamond-like cubic BN (c-BN) are four crystal forms of BN [96]. There are two kinds of hybrid methods including $sp^2$ and $sp^3$ hybridization. Among them, w-BN and c-BN are low-density phases with $sp^3$ hybridized bonds; however, r-BN and h-BN are dense phases with $sp^2$ hybridized B-N bonds [51, 96]. The crystal structure parameters of boron nitride were shown in Table 2. In the recent publications, the two-dimensional h-BN nanosheets not only have the unique layered structure of graphene, but also have the unique properties of high surface areas, non-toxicity, low density and high chemical stability, which have attracted a great deal of attention [46]. Many researchers showed that BN/semiconductor nanomaterials such as BN/$TiO_2$ [141], BN/g-$C_3N_4$ [46] and BN/ZnO [142] could be regarded as a promising catalyst for the heterogeneous photocatalysis. Hence, h-BN was reported to be a robust substrate for semiconductor photocatalysts owing to its optical properties, electrical properties and hydrogen storage properties. In order to understand the applications and interaction mechanism of BN-based and BN nanomaterials, it was vital to study their electronic and optical properties [143].

#### 3.2.1 Optical properties

Bare h-BN single crystals manifest a series of s-like exciton absorption bands

Accepted MS

about 215 nm and a dominant luminescence peak under high-temperature and high-pressure [144]. In a similar pattern, h-BN nanosheets exhibit strong cathodoluminescence (CL) emission in the deep ultraviolet range [104, 145].The representative CL spectrum of the BNNSs was depicted in Fig. 6a, it exhibits broad emission band centered about 265 nm. Fig. 6b also exhibits the representative CL spectra of granular BN films, which show centered around 360 nm in the range of 260~520 nm [145]. Owing to this property, 2D h-BN nanomaterial was a “rising star” for ultraviolet optical devices. Furthermore, h-BN may have a number of applications such as hydrogen storage, ophthalmic surgery, photocatalysis and sterilization [51, 144].

Similar to CL spectra, the Raman spectrum characteristic peaks of h-BN nanosheets are also equivalent to those of the bulk counterpart [115, 146]. The general Raman characteristic peaks of h-BN nanosheets were within range of 1364–1368 $cm^{-1}$ (about 1365 $cm^{-1}$), which belongs to the B–N high-frequency vibrational mode ($E_2g$) and analogous to the Raman shift in bulk h-BN single crystals (1366 $cm^{-1}$) [51, 115, 145]. The representative FTIR and Raman spectrum of the BNNSs is shown in Fig. 6c and Fig. 6d. In Gorbachev’s study, the mutual effect between neighboring nanosheets in few-layer h-BN and growth temperature-induced variation of crystalline nature lead to red shifts of Raman spectra. On the contrary, single-layer h-BN which has a mildly shorter B–N bond could render blue shifts of Raman spectra [147].

### 3.2.2 Electronic properties

Accepted MS

Different from carbon nanomaterials, unmodified 2D BN nanostructures such as nanotubes, nanosheets and nanoribbons show insulator characteristics with a wide bandgap in the range of 5.0–6.0 eV. There were various methods to effectively modify band-gap of BN nanostructures, and the common one was doping a third element (i.e. carbon) into their nanostructures [148-150]. Recently, many studies revealed that a mixture of N, C and B atoms forms a more stable structure than pure h-BN and graphene [148]. Hence, Boron carbonitride ($B_xC_yN_z$) nanostructures become very popular in electronic field because of their semiconductor-like properties. As mentioned above, the band gap of bare h-BN nanosheets is 5.66 eV [148, 149], while BN–C compound showed much smaller band gaps, 1.25 eV due to incorporation of C in BN domains.

**3.3 N-doped**

In addition to graphite carbon nitride and boron nitride, N-$TiO_2$ and other N-dopant is also the representative of nitride and N-doped photocatalysts family. $TiO_2$ is a popular nanomaterial for photocatalysis applications owing to its high stability, low toxicity and low cost, but it is active only under the UV light [58, 61, 151]. A breakthrough work about nitrogen doping $TiO_2$ for photocatalysis application of photo-degradation of pollution (methylene blue) was reported in 2001 [62]. After that, there are many researches on the nitrogen doping $TiO_2$. For example, Pablos et al. successfully prepared nitrogen doped $TiO_2$ nanotubes by anodizing Ti foil, and the as-prepared materials possess excellent UV-Vis activity [152]. Other photocatalyst (NiO, ZnO, $(BiO)_2CO_3$ etc) mixed with nitrogen materials could also improve the

Accepted MS

property of electron transport and suppress electron−hole recombination [153, 154]. For instance, Keraudy and his team had synthesized N-doped nickel oxide (N-NiO) via reactive magnetron sputtering method in gas atmosphere of $N_2/O_2/Ar$, and some testing tools revealed the final product exhibited good performance [153]. ZnO is a semiconducting material with 3.2 eV band gap, it has wurtzitetype hexagonal crystal structure [155-157]. In Narayanan's paper, authors tried to prepare N-doped ZnO to further enhance its photocatalytic activity via spray pyrolysis method . Crystallinity of N-doped ZnO thin films was deteriorated, which might cause increased absorption losses and increase in scattering of photons. The bandgap energy of N-doped ZnO got narrowed with N concentration increased, which might caused by localization of impurity levels in the forbidden gap near the valence band edge in the ZnO lattice [155]. Particularly, consider the limited application of pure $(BiO)_2CO_3$, nitrogen element doping have been utilized to enhance its photocatalytic efficiency [158-161]. The introduction of nitrogen element could upshift the VB position of $(BiO)_2CO_3$. Combined DFT calculations and experimental results, Dong and coworkers prepared N-doped $(BiO)_2CO_3$ with narrowed band gap and superior photocatalytic activity [161].

Accepted MS

## 4. Catalysis applications in water splitting

Producing clean and sustainable hydrogen energy is an important prerequisite for the future development of the hydrogen energy economy. By water electrolysis from renewable resources and the direct solar photochemical water splitting into hydrogen

transformation is a promising pathway to achieve sustainable hydrogen production [162, 163]. To mimic the natural photosynthesis, the materials of nitride family are prepared for photocatalysis water splitting into oxygen ($O_2$) and hydrogen ($H_2$). Nevertheless, most of researchers have studied the half reaction of water splitting, mainly the production of $H_2$ [78]. The photocatalysts for hydrogen generation must meet certain conditions: (1) the position of the semiconductor catalyst conduction band (CB) is negative to the potential of $H_2/H_2O$, and the valence band (VB) position is at the potential of $O_2/H_2O$. (2) The band gap of semiconductor catalyst is greater than the cracking voltage of water 1.23 eV.

**4.1 g-$C_3N_4$**

Wang et al. firstly used g-$C_3N_4$ as photocatalyst in 2009, and they observed an efficient $H_2$ production by using visible light irradiation [164]. On the basis of that, g-$C_3N_4$ has dramatically attracted research interest [165-168]. Wang and his coworkers prepared the mesoporous g-$C_3N_4$ by the template method and the resulted sample enhanced nearly 8-folds for photocatalytic $H_2$ evolution than bulk g-$C_3N_4$ [165]. Very recently, Zhang and coworkers used SBA-15 as the template synthesis of the ordered mesoporous CN (ompg-CN). The optimized ompg-CN exhibits a commendable photocatalytic activity towards hydrogen evolution which could reach 290 μmol $h^{-1}$ [166]. Zhao et al. have found that a facial, one-step soft templating method to synthesize the hollow g-$C_3N_4$ nanospheres with more porosity and bigger surface area. To study the photocatalytic performance of as-prepared materials, the hydrogen evolution experiments were carried out. Especially, the sample CN-$E_{0.08}$

Accepted MS

(ethanol carbon nitrogen) shows the highest hydrogen production, as high as 157 umol $h^{-1}$ [167]. Niu and coworkers successfully prepared g-$C_3N_4$ nanosheets with ~2 nm thickness via a thermal oxidation etching process, and the $H_2$ evolution rate of nanosheets reaches 170.5 μmol $h^{-1}$ under VLD irradiation [168]. These studies showed that researchers could control g-$C_3N_4$ nanostructure to enhance the photocatalytic activity of g-$C_3N_4$ photocatalysts.

However, there are still much room to improve the bare g-$C_3N_4$ efficiency because of low sunlight absorption and unsatisfactory charge separation [169-171]. Element doping is known to be a promising method to control the electronic properties and structure of g-$C_3N_4$ to obtain enhanced performance [67]. Huang et al. described a new precursor reforming strategy to prepare 3D porous ultrathin N self-doped g-$C_3N_4$ products, which exhibits ~3 nm thickness sheets (7 or 8 layers). The optimum photocatalyst UM3 (the molar ratio of urea:melamine=3:1) yields hydrogen evolution rate of 700 μmol $h^{-1}$, which was far superior to that of the bulk counterpart obtained by direct melamine calcination (17 μmol $h^{-1}$) [172]. Another interesting observation is that N-doped graphitic carbon-incorporated g-$C_3N_4$ (denoted as N-g-$C_3N_4$) exhibits better photo-catalytic property compared with pure g-$C_3N_4$. Zhou et al. use a simple one-pot method to obtain N-g-$C_3N_4$, which the generation rate of $H_2$ was about 4.3 times on bulk g-$C_3N_4$ [173, 174]. In this composite, the N atom mainly work for extended and delocalized aromatic p-conjugated system of g-$C_3N_4$ and remarkably enhanced photocatalytic $H_2$ evolution activity [173].

**4.2 BN based and N-doped**

Accepted MS

Hexagonal boron nitride was extensively researched and applied in the photocatalysis fields. However, the band-gap of h-BN was about 5.5 eV, which was not suitable for photocatalytic $H_2$ evolution [175, 176]. Coincidentally, graphene nanomaterial cannot directly absorb the light energy because of its zero band-gap, and its further applications of photocatalytic were restricted [177]. Hence, it is desirable to constitute medium-bandgap photocatalyst including h-BN and graphene (or carbon), which shows better properties and tunable electronic structure system. Wang's group prepared boron carbon nitride tubes (introduced C into h-BN) via a facile and novel biotemplating method with using kapok fibers (carbon sources and templates) [178]. In this work, the boron carbon nitride tubes-2 sample shows the highest hydrogen evolution rate (2.8 μmol $h^{-1}$). As depicted in Fig. 7a, with the carbon content in BCNTs further increases, the hydrogen evolution rate of photocatalytic performance gradually decreases. The catalytic stability of as-prepared sample was shown in Fig. 7b. Furthermore, the morphology of boron carbon nitride tubes-2 was also shown in Fig. 7c and Fig. 7d. Moreover, based on carbon doping, Huang and his team had synthesized a ternary catalytic of BCN nanosheets with a narrowed band-gap (2.0 eV), and the BCN nanomaterials could be excited by visible light [179]. The best performance of $H_2$ evolution was BCN-30, its reactivity was maintained for about 100 h, which indicates an excellent chemical stability and its quantum efficiency reached 0.54% at 405 nm wavelength through calculation.

The pioneering works in hydrogen production field about $TiO_2$ photocatalysis were performed by Fujishima and Honda in 1972 [180]. Since then, N doped $TiO_2$

Accepted MS

photocatalyst has attracted global interest for hydrogen production under solar irradiation owing to its stable chemical properties and unique photoelectric [181, 182]. Shim et al. found a novel method to prepared N-$TiO_2$ with anatase/rutile/brookite mixed phases in urea aqueous solution [181]. In this paper, the sample NTU-2.5 (anatase: rutile: brookite = 69%: 14%: 17%) showed the highest photoactivity of hydrogen yield of 10500 mmol/h/g relative to other photocatalysts tested such as P25 (commercial $TiO_2$) and NTU-0 (pure anatase).

For other N doped catalysis, Carbon quantum dots (CQDs) can be an appropriate choice due to quantum confinement effects, proper band-gap and excellent electron donor/acceptor properties [182, 183]. Shi and co-workers fabricated N-doped carbon quantum dots (NCDs)/$TiO_2$ photocatalysts via a facile hydrothermal method for photocatalytic hydrogen evolution [182]. As shown in Fig. 8a and Fig. 8b, Shi et al. studied the efficiency of hydrogen production under different light illumination conditions. Under VLD illumination, $H_2$ evolution rates were 58.6, 27.1, 21.2 and 0 nmol $h^{-1}$ for NCDs-3/P25, NCDs-2/P25, NCDs-1/P25 and bulk P25 ($TiO_2$), respectively. When the light condition was full spectrum illumination, NCDs-3/P25, NCDs-2/P25, NCDs-1/P25 and bare P25 can generate 9.80, 5.12, 2.70 and 1.15 μmol $H_2$ each hour, respectively. It is evident that N-doped carbon quantum dot express much better photocatalytic performance than P25 under both full spectrum and visible light [182]. The photocatalytic stability test under full spectrum is shown in Fig. 8c, and a plausible mechanism of photocatalytic $H_2$ evolution is described in Fig. 8d. On the basis of data presented herein, NCDs could regard as both electron reservoirs and

Accepted MS

photo-sensitizers in NCDs/P25 composites. In addition, Jing et al. used template-free method to prepare three different morphologies (nanoparticles, nanorods and nanobelts) N-$MoC_2$ for hydrogen evolution reaction [184]. The favorable HER catalytic performance might be caused by heteroatom N, because the existence of pyridinic N, charge density distribution and asymmetry spin could enhance the interaction with $H^+$. Ulteriorly, the nitrogen dopants could possess strong electron-withdrawing features, thus making the neighboring carbon atoms to play dual roles both as electron acceptors and electron donors [184-186].

Accepted MS

## 5. Photocatalytic degradation of pollutants

As the economy continues to develop, we face a huge environmental problem since widespread effluents and gaseous pollutions enter into human society [26, 187-196]. In recent decades, many scientific researchers made a large quantity of effort to solve the above problem, among many methods, photocatalytic technology attains widely attention and has been applied in environmental conservation due to its simple, economic and feasible [68, 197-201].

### 5.1 g-$C_3N_4$

In 2009, Wang and his coworkers used the g-$C_3N_4$ as photocatalysts for photocatalytic hydrogen evolution [164]. Since then, g-$C_3N_4$ has quickly become a hotspot in the field of photocatalysis and it was extensively used in environmental applications including water decontamination and air purification. However, bare g-$C_3N_4$ was rarely used in photocatalysis field because of its insufficient solar light

absorption and low efficient of degradation pollutants. Hence, g-$C_3N_4$-based semiconductor photocatalysts have been extensively applied to photocatalytic degradation of environmental pollutants [58, 202-204]. (Fig. 9) Generally, the photocatalytic degradation of pollutants with modified g-$C_3N_4$ showed in researches can be classified into two categories: liquid-phase removal of contaminants and gas-phase degradation of pollutants mainly about $NO_x$ [202, 205-208]. G-$C_3N_4$ dopant photocatalysts and their photocatalytic performances are shown in Table 3.

**5.1.1 Liquid-phase degradation of pollutants**

Among the organic contaminants that evaluated the photoactivity of the catalyst, dyes [209-211], tetracycline (TC) [212-215] and other antibiotics [190, 216-219] were most widely used in water. For instance, Dong et al. fabricated inorganic–organic composites comprised of VLD photocatalyst of CdS and g-$C_3N_4$ via a precipitation–deposition method. The optimum photocatalyst 0.7g-$C_3N_4$-0.3g-CdS was almost 3.1 and 20.5 times higher than pure CdS and g-$C_3N_4$ toward remove dye of methyl orange (MO), respectively [203]. Zou and coworkers prepared bulk g-$C_3N_4$ and boron-doped g-$C_3N_4$ (BCN) via heating melamine and the mixture of melamine and boron oxide, respectively. Optimum BCN sample possessed the highest degrading rate of RhB which was approximately 1.5-fold faster than RhB photodegrading over the bulk g-$C_3N_4$ prepared at the uniform conditions [210]. Katsumata et al. prepared a highly efficient g-$C_3N_4$/$Ag_3PO_4$ Z-Scheme photocatalysts by situ precipitation method. Among the hybrid photocatalysts, best hybrid sample revealed the highest photocatalytic activity which took only five min of VLD irradiation for the total

Accepted MS

remove of 10mg/L MO [211]. The photocatalytic activity of g-$C_3N_4$, $Ag_3PO_4$ and g-$C_3N_4$/$Ag_3PO_4$ compound photocatalysts on the degradation of MO was shown in Fig. 10a.

Because of widely distribution in water resource and unique difficult decomposing of antibiotic, many researchers use TC as target pollutions to explore the photocatalytic properties of materials [220]. For instance, Chen et al. successfully prepared a three-component heterojunction photocatalyst (Bi/α-$Bi_2O_3$/g-$C_3N_4$, labeled as BBC) which Bi/α-$Bi_2O_3$ nanoparticles loading on g-$C_3N_4$ nanosheets via a calcination photoreduction technique. BBC showed a remarkably high photocatalytic performance under VLD irradiation, the degradation rate reached almost 90.2% for TC [212]. In Wang's study, they developed a facile method to immobilize 2D/2D structured g-$C_3N_4$/rGO hybrid coating on 3D nickel foam so as to enhance the phtocatalytic performance and cyclic stability of g-$C_3N_4$ [213]. Because of the abundant coupling heterointerfaces between rGO and g-$C_3N_4$ in this hybrids, the recombination of light induced $h^+/e^-$ were hugely suppressed and the 2D/2D structured g-$C_3N_4$/rGO compound coating on 3D nickel foam demonstrated the superior photocatalytic performance. In the photocatalytic test, CN-9 (weight ratio of g-$C_3N_4$ nanosheets to GO) sample demonstrates the highest degradation efficiency (90%) [213]. The mechanism of g-$C_3N_4$/rGO coatings immobilized on nickel foam was shown in Fig. 10b and the XRD patterns of g-$C_3N_4$/rGO materials were depicted in Fig. 10c.

Accepted MS

Antibiotics are another target pollutants, their resistance has become more and more evident. And antibiotics could be detected in soils, sediment, aqueous system and even the food on our table [216, 217]. Dr. Xiao's team synthesized a promising g-$C_3N_4$/$WO_3$ heterojunction hollow microsphere by in situ hydrolysis and polymerization, and the as-prepared materials showed high photocatalytic activity for removal ceftiofur sodium (CFS) under VLD irradiation. The optimal sample exhibited the highest degradation efficiency (82%) of CFS after 120 min of VLD irradiation [216]. Zhang et al. constructed a 0D/2D heterojunctions of $Bi_3TaO_7$ quantum dots /ultrathin g-$C_3N_4$ nanosheets via an economical sol-gel method. The best sample of 20 wt% g-$C_3N_4$ NSs has excellent photocatalytic performance for the degradation of ciprofloxacin, and its photocatalytic efficiency was 12.2 times and 4 times that of pure g-$C_3N_4$ and $Bi_3TaO_7$, respectively [217].

**5.1.2 Gas-phase degradation of pollutants**

$NO_x$ including $NO_2$ and NO has been one of main air pollutants [202]. $NO_x$ can cause atmospheric pollutions like urban smog and acid rain which were harmful for human health. Therefore, removing $NO_x$ is a challenging task nowadays. As a big photocatalyst family of nitride, g-$C_3N_4$-based gives a new avenue for this research [221, 222]. In order to solve bulk g-$C_3N_4$ problem of high recombination of light-induced carriers and small surface area, Li and coworkers prepared mesoporous g-$C_3N_4$ (MCN) mix with graphene oxide (GO) and graphene (G) to remove NO [223]. The MCN-G showed a NO removal efficiency of 64.9%, which was better than that of bare g-$C_3N_4$ (16.8%) and MCN-GO (60.7%), confirming that porous g-$C_3N_4$ and

Accepted MS

graphene have a synergistic effect to improve the photocatalytic performance [223]. Qu et al. designed a hierarchical g-$C_3N_4$@Ag/$BiVO_4$ (040) hybrid photocatalyst which exhibited higher photocatalytic performance for NO oxidation with respect to pristine $BiVO_4$ and bulk g-$C_3N_4$ [224]. In this paper, the reason of the high performance for removing NO was the efficient generation of $h^+$, $^{\cdot}O_2$, $^{\cdot}OH$, and $^{\cdot}OH$ plays a vital role [224]. Owing to the property of resistance to oxygen of g-$C_3N_4$, it makes g-$C_3N_4$ decompose NO can be reacted in the presence of NO, and there are no negative effects for photocatalysts. Compared to other photocatalyst, g-$C_3N_4$ have a bright future and huge potential in NO decomposition [222].

**5.2 BN based and N-doped**

Boron nitride nanomaterials has special chemical stability, extreme large surface area and high thermal conductivity, and demonstrates advantages in water cleaning [96]. This section presents the BN or BN-modified photocatalysts for the degradation of diverse contaminants from water. BN-based photocatalysts and their photocatalytic performances are shown in Table 4.

For the degradation of dye, Wu et al. prepared composites $Ag_2CrO_4$/few layer boron nitride via a situ precipitation method [225]. In this paper, the as-prepared $Ag_2CrO_4$/FBNNS-10wt% exhibited the highest photocatalytic activity of 96.7% higher than 75% of pure $Ag_2CrO_4$. Similarly, Song et al. synthesized graphene-analogues BN modified $Ag_3PO_4$ photocatalysts, and the 0.5 wt% BN/$Ag_3PO_4$ composite presented the optimum photocatalytic performance [226]. BN can improve other photocatalyst charge separation ability and enhanced

Accepted MS

photocatalysis ability. Very recently, for broaden the absorption spectrum, Weng et al. prepared BN mesoporous nanosheets (BNPS) with richly exposed (002) plane edges by a simple method and the materials exhibit wide-spectrum light absorptions [227]. The photocatalytic performances of $TiO_2$/BNPS composites were evaluated via photocatalytic oxidation of organic compounds (acetic acid and crystal violet) to evolve $CO_2$ in aqueous solutions, and compared to P25 ($TiO_2$). The photocatalytic performances of composites were shown in Fig. 11.

N-doped nanomaterials such as N-$TiO_2$ [228-231], N-ZnO [232, 233] and N-CQDs [234, 235] have made a great contribution to the removal of organic pollutants in water due to theirs chemical stability and good optical property. Very recently, Liu and their teamworkers developed a heterojunction composites N-doped $KTiNbO_5$/g-$C_3N_4$ (NTNO/CN) via one-step calcination approach [236]. The NTNO/CN photocatalysts exhibited excellent photocatalytic activity for degradation of rhodamine B and bisphenol A. It is noted that the layered heterojunction and N doping has synthetic effect to improve the efficiency of light harvesting and charge separation of NTNO/CN. During the photocatalytic process of RhB degradation, the active species of $\bullet O_2^-$ played a dominated role and $h^+$ played an assistant role [236]. Similarly, Peter et al. used coprecipitation and wet chemical method to prepared N-doped ZnO/GO (NZGO), and their photocatalytic activity were evaluated by the degradation of brilliant smart green (BG) dye [237]. The lattice constants, the cell volume, and the crystalline size of N-ZnO are smaller than ZnO, which might caused by nitrogen occupies interstitial positions of crystal lattice. Thus N-ZnO shows a

Accepted MS

higher photocatalytic activity than pure ZnO under visible light irradiation. Many other N-doped photocatalysts and their photocatalytic performances of degradation of organic pollutants were shown in Table 5.

## 6. Photocatalytic carbon dioxide reduction

As one of the reasons causing the global climate change, greenhouse gas carbon dioxide ($CO_2$) has now become a global environmental issue because of fossil fuel abundant consumption. In the foreseen future, energy shortage and environmental pollution have become two main problems [189, 238-241]. Solar energy is considered to be the most important sustainable energy source. Therefore, it is of significant importance to efficiently and inexpensively convert solar energy into chemical fuels by manual method [242].

Photocatalytic reduction of $CO_2$ is known as a challenging but promising application for energy utilization to settle the climate change and energy crisis in the near future [68]. The pioneer work of photocatalytic reduction of $CO_2$ was made by Honda and coworkers, who studied various semiconductor photo-catalysts transformation efficiency and photo-degradation products [243]. $CO_2$ can be converted into formic acid (HCOOH), methanol ($CH_3OH$), CO, methane ($CH_4$), and formaldehyde (HCHO) during the photocatalytic process [244]. The possible products from $CO_2$ reduction depending on the different reaction mechanisms and pathways are shown in Table 6 [245, 246].

### 6.1 g-$C_3N_4$

Accepted MS

As a member of nitride and N-doped materials family, g-$C_3N_4$ was a metal free, low-cost and great visible light adsorbing potential semiconductor, which has been proven to be the appropriate photocatalytic material since its CB and VB are positioned at −1.14 eV and 1.57 eV, respectively. Clearly, the CB location of g-$C_3N_4$ was adequately negative to transform $CO_2$ [244]. Owing to the fast recombination of light-induced $h^+/e^-$, it still exist some problems photocatalytic reduction of $CO_2$ by using bare g-$C_3N_4$.

Many researchers paid their efforts to overcome this issue. For example, Wang et al. synthesized conjugated g-$C_3N_4$ nanosheets modified with barbituric acid via a simple chemical condensation of urea [247]. In this study, the best sample (CNU-$BA_{0.03}$) showed 15-fold-enhanced photocatalytic performance for the $CO_2$-to-CO conversion reaction compared to the bulk CNU (non-modified) material. After four hours reaction, 56.3 μmol CO were obtained from the reaction system with the help of CNU-$BA_{0.03}$ [247]. In the other aspect, Wang and colleagues synthesize noble-metal-free system by integrating g-$C_3N_4$ with a cobalt-containing zeolitic imidazolate framework (Co-ZIF-9), this hybrid system significantly enhanced $CO_2$-to-CO conversion efficiency under VLD illumination. Among them, Co-ZIF-9 showed various functions in promoting photo-generated charge separation and $CO_2$ adsorption [244, 248].

In addition to CO, $CO_2$ also can be converted into many other chemicals and fuels including $CH_4$, $CH_3OH$, HCOOH and HCHO. In Mao's study, they synthesized two kinds of g-$C_3N_4$ via a thermal decomposition process of urea or melamine, and

Accepted MS

denoted as u-g-$C_3N_4$ or m-g-$C_3N_4$. They found an interesting phenomenon that $CO_2$ can be converted into $C_2H_5OH$ when m-g-$C_3N_4$ was photocatalyst, while u-g-$C_3N_4$ leads to a mixture including $C_2H_5OH$ and $CH_3OH$ [249]. This phenomenon was possibly caused by the different crystallinity and microstructure of the two kinds of g-$C_3N_4$. Moreover, Yu et al. used a simple calcination method to constructed binary Z-scheme of g-$C_3N_4$/ZnO, and applied it for the photocatalytic converted of $CO_2$ into $CH_3OH$ [250]. Maeda et al. prepared a promising heterogeneous photocatalyst system with ruthenium complex based on g-$C_3N_4$, this hybrid material realized the high selectivity for HCOOH production which can maintained HCOOH 67.7 mmol with 20 hours. Therefore, Maeda's research clearly demonstrates the potential of carbon dioxide-based multiphase photocatalysts to reduce carbon dioxide using solar energy [251]. The photocatalysis of $CO_2$ reduction by using a Ru complex/$C_3N_4$ hybrid was illustrated in Fig. 12, along with structures of the used Ru complexes. By doping g-$C_3N_4$ with elemental photocatalyst red phosphor, Xue and coauthors also found that an enhanced $CH_4$ production by $CO_2$ photoreduction under 500W xenon arc lamp irradiation. In their study, optimal red phosphor/g-$C_3N_4$ hybrids (PCN-30) exhibited a $CH_4$ production yield of 295 mol $h^{-1}$ $g^{-1}$, which was twice higher than bare red phosphor (145 mol $h^{-1}$ $g^{-1}$) and approximately enhanced three times than bare g-$C_3N_4$ (107 mol $h^{-1}$ $g^{-1}$) [252].

**6.2 BN based and N-doped**

Compared to g-$C_3N_4$, BN and N-doped photocatalysts research in photocatalytic reduction of $CO_2$ was very rare. The reason of this phenomenon was that hexagonal

Accepted MS

BN has a wide band-gap (5.5 eV) and its light absorptions is negligible when the light wavelength is above 300 nm [253]. For nitrogen doped $TiO_2$, Akple et al. fabricated nitrogen-doped anatase $TiO_2$ microsheets (N-$TiO_2$ MS) via a hydrothermal method with the help of HF and HCl [254]. In this paper, the N-$TiO_2$ MS sample exhibited a much better property than its precursor TiN and P25 (commercial $TiO_2$) for photocatalysis $CO_2$ reduction. The detected product from as prepared materials is $CH_4$, $CH_3OH$ and $CH_2O$. Besides, Oliveira et al. used urea as a nitrogen precursor to obtained N-doped ZnO, and the N-ZnO showed outstanding performance for $CO_2$ photoreduction [156]. In this work, $CH_4$ was the only product of $CO_2$ photoreduction reaction, and the $CH_4$ production rate of optimal sample was about 0.23 mol $L^{-1}g^{-1}h^{-1}$. Similarly, Núnez et al, prepared ZnO:N nanoparticles and used the samples for photocatalysis $CO_2$ reduction under UV irradiation, and the final product were $H_2$, CO, $CH_4$, and $CH_3OH$ [255]. Although the reduction of $CO_2$ via BN based and N-doped photocatalysts was in the early stages of development, it still was a very promising direction worthy of research.

Accepted MS

## 7. Theoretical advances on nitride and nitrogen-doped photocatalysts

With the development of nanomaterials, the system of nanomaterials is more and more complicated, and the traditional analytical derivation method is insufficient [256, 257]. Fortunately, the theoretical calculations relying on computer simulation provide a new means for the study of complex systems. The combination of theoretical calculations and experimental research has become the inevitable result of scientific

progress [258]. For photocatalysis, Density functional theory (DFT) may explain the possible photo-induced charge transfer within photocatalytic process which is fundamental to guide the modification of the photocatalysts nanomaterials [259-261]. Therefore, it is necessary to understand the theoretical advances on nitride and nitrogen-doped photocatalysts.

Based on results of DFT calculations, the tri-s-triazine-based structure of g-$C_3N_4$ was proved the most stable structure [262]. In order to further explore the catalytic mechanism of g-$C_3N_4$ (mainly to clarify the position of catalytic active sites), the lowest unoccupied orbit (LUMO) and the highest occupied orbit (HOMO) of monolayer g-$C_3N_4$ are given, as depicted in Fig. 13a and Fig. 13b [263, 264]. It should be noted that HOMO is mainly composed of N 2p orbits with weak in-plane coordination, while LUMO is mainly composed of C 2p orbits in the Z-axis direction [265, 266]. The distribution of HOMO and LUMO tends to a low coordination N atom and edge C atoms, respectively [267]. Moreover, no $e^-$ would be excited from bridge N (N3) atoms under visible light, and the lightgenerated $e^-$ can neither migrate to N3 atoms nor transfer from one heptazine ($C_6N_7$) unit to the adjacent unit through N3 atoms, resulting the separation efficiency of photogenerated carriers of bare g-$C_3N_4$ is inefficient [263]. Therefore, the computational study of HOMO and LUMO provides a favorable theoretical basis for the strategy of enhancing the photocatalytic activity of g-$C_3N_4$ [268, 269].

The 2D h-BN is a particularly attractive nanomaterial and has drawn intensive interest due to its unique structure, stability and low cost [270]. Based on results of

Accepted MS

DFT calculations, the band structure and electron density of h-BN were shown in Fig. 13c and Fig. 13d [271]. It is easy to find that the VB edge of h-BN is mainly composed of N 2p and N 2 s orbits, and the CB edge of h-BN is basically composed of B 2p orbit. The nitrogen atoms of VB have a lower hybridization with the adjacent boron atoms, which indicats that $e^-$ of VB are easily to be excited [271-273]. Based on the fact that nitrogen doping is a good strategy for adjusting the electronic structure and enhancing the photocatalytic performance of semiconductor, there are also many theoretical studies and experimental scenarios on nitrogen-doped photocatalysts [61, 154]. For example, Dong et al. prepared a visible light driven N-doped $(BiO)_2CO_3$ photocatalyst via a facile green route, and the role of N atoms was revealed by DFT calculations [161]. The nitrogen atoms are doped into the crystal structure for upward shift VB top of $(BiO)_2CO_3$, resulting in narrowed bandgap and boost the visible light absorption. Similar results have also been discovered in Peng's work, the DFT results indicate that nitrogen doping can produce vacant states above the Fermi level and shift the CB into lower energy region, resulting in a stronger light absorption of N-doped ZnO [274]. In brief, the theoretical investigations on nitride and nitrogen-doped photocatalysts may shed light on the fundamental understanding of the underlying mechanism.

Accepted MS

## 8. Conclusions and perspectives

The new family of nitride and N-doped nanomaterials covers a wide range of physicochemical properties for the applications in environment and energy. However,

compared to carbon-based photocatalysts, the nitride materials are barely described in reviews, and their economic potential (energy aspect) and photocatalytic performance (environment aspect) are fully covered. The models of nitride and N-doped materials are BN, g-$C_3N_4$, N-$TiO_2$ and other N-dopants, most of them have the ability to solve problem of energy crisis. In this review, the preparation methods of nitride photocatalysts are firstly discussed. Then the properties of nitride photocatalysts (optical and electronic) and the catalysis applications of nitride photocatalysts are also showed. In conclusion, this critical review summarizes family of nitride and N-doped preparation, properties and applications in hydrogen evolution from water, environmental pollutants removal and carbon dioxide reduction etc.

Many researchers studied the representatives of nitride and N-doped photocatalysts and achieved significant progress, but the researches in photocatalysis field were still needed further systematic investigation and there were many challenges in the future development studies: (1) One of awkward challenges we met is the nonrepeatability of photocatalysts fabrication. From buy raw materials to construction of precursor and final product, from calcination materials to any experimental operation, none of the unified standard is listed, and neither specification of experimental instrument nor the unified presentation of technological process and synthesis process were introduced. (2) Density functional theory (DFT) can indicate a way for practice of photocatalysts. However, to our best knowledge, the quantitative calculation is barely applied to demonstrate the relationship between photocatalytic efficiency and quantum yield of photocatalysts. Moreover, DFT may

Accepted MS

explain the possible photo-induced charge transfer within photocatalytic process which is fundamental to guide the modification of the photocatalysts nanomaterials. (3) The mechanisms of photocatalytic improvement by the nitride semiconductor systems are partly unclear. For instance, a photocatalyst which is more effective in removing contamination may exhibit poor performance in the process of generating hydrogen from water or carbon dioxide reduction. Also, it is indispensable to develop a uniform method to evaluate the photocatalytic property because of current diverse evaluation methods. (4) Although some researches about quantum dots are ongoing, we should further developed nitride photocatalysts quantum dots.

The prospect of nitride photocatalysts looks bright. Continued progress in this field will overcome the above challenges, and to develop a class of photocatalysts with excellent selectivity and superior photosensitivity for a wider range of applications.

Accepted MS

**Acknowledgements**

This study was financially supported by the Program for the National Natural Science Foundation of China (51879101, 51579098, 51779090, 51709101, 51278176, 51521006, 51378190, 51809090, 51278176, 51408206, 51508177), the National Program for Support of Top-Notch Young Professionals of China (2014), the Fundamental Research Funds for the Central Universities, Hunan Provincial Science and Technology Plan Project (No.2016RS3026, 2017SK2243，2018SK20410), the Program for Changjiang Scholars and Innovative Research Team in University

(IRT-13R17)，and the Fundamental Research Funds for the Central Universities (531109200027, 531107050978, 531107051080).

## References

[1] Zhou C, Lai C, Xu P, Zeng G, Huang D, Zhang C, et al. In Situ Grown AgI/$Bi_{12}O_{17}Cl_2$ Heterojunction Photocatalysts for Visible Light Degradation of Sulfamethazine: Efficiency, Pathway, and Mechanism. ACS Sustain. Chem. Eng. 2018;6(3):4174-84.

[2] Xiong W, Zeng G, Yang Z, Zhou Y, Zhang C, Cheng M, et al. Adsorption of tetracycline antibiotics from aqueous solutions on nanocomposite multi-walled carbon nanotube functionalized MIL-53 (Fe) as new adsorbent. Sci. Total Environ. 2018;627:235-44.

[3] Xiong W, Tong J, Yang Z, Zeng G, Zhou Y, Wang D, et al. Adsorption of phosphate from aqueous solution using iron-zirconium modified activated carbon nanofiber: Performance and mechanism. J. Colloid Interface Sci. 2017;493:17-23.

[4] Cheng M, Zeng G, Huang D, Lai C, Xu P, Zhang C, et al. Degradation of atrazine by a novel Fenton-like process and assessment the influence on the treated soil. J. Hazard. Mater. 2016;312:184-91.

[5] Yang Y, Zeng Z, Zhang C, Huang D, Zeng G, Xiao R, et al. Construction of iodine vacancy-rich BiOI/Ag@AgI Z-scheme heterojunction photocatalysts for visible-light-driven tetracycline degradation: Transformation pathways and

Accepted MS

mechanism insight. Chem. Eng. J. 2018;349:808-821.

[6] Xu P, Zeng GM, Huang DL, Feng CL, Hu S, Zhao MH, et al. Use of iron oxide nanomaterials in wastewater treatment: A review. Sci. Total Environ. 2012;424:1-10.

[7] Tang W-W, Zeng G-M, Gong J-L, Liang J, Xu P, Zhang C, et al. Impact of humic/fulvic acid on the removal of heavy metals from aqueous solutions using nanomaterials: A review. Sci. Total Environ. 2014;468:1014-27.

[8] Tan X, Liu Y, Zeng G, Wang X, Hu X, Gu Y, et al. Application of biochar for the removal of pollutants from aqueous solutions. Chemosphere. 2015;125:70-85.

[9] Huang D, Hu C, Zeng G, Cheng M, Xu P, Gong X, et al. Combination of Fenton processes and biotreatment for wastewater treatment and soil remediation. Sci. Total Environ. 2017;574:1599-610.

[10] Huang D, Xue W, Zeng G, Wan J, Chen G, Huang C, et al. Immobilization of Cd in river sediments by sodium alginate modified nanoscale zero-valent iron: Impact on enzyme activities and microbial community diversity. Water Res. 2016;106:15-25.

[11] Xie L, Bai Y, Qi Y, Wang H. Pultruded GFRP square hollow columns with bolted sleeve joints under eccentric compression. Compos B Eng. 2019;162:274-82.

[12] Lai C, Liu S, Zhang C, Zeng G, Huang D, Qin L, et al. Electrochemical Aptasensor Based on Sulfur-Nitrogen Codoped Ordered Mesoporous Carbon and Thymine-Hg(2+)-Thymine Mismatch Structure for Hg(2+) Detection. ACS Sens. 2018.

[13] Huang D, Liu L, Zeng G, Xu P, Huang C, Deng L, et al. The effects of rice straw biochar on indigenous microbial community and enzymes activity in heavy

Accepted MS

metal-contaminated sediment. Chemosphere. 2017;174:545-53.

[14] Xue W, Huang D, Zeng G, Wan J, Zhang C, Xu R, et al. Nanoscale zero-valent iron coated with rhamnolipid as an effective stabilizer for immobilization of Cd and Pb in river sediments. J. Hazard. Mater. 2018;341:381-389.

[15] Huang D-L, Wang R-Z, Liu Y-G, Zeng G-M, Lai C, Xu P, et al. Application of molecularly imprinted polymers in wastewater treatment: a review. Environ. Sci. Pollut. Res. Int. 2015;22(2):963-77.

[16] Gong X, Huang D, Liu Y, Zeng G, Wang R, Wei J, et al. Pyrolysis and reutilization of plant residues after phytoremediation of heavy metals contaminated sediments: For heavy metals stabilization and dye adsorption. Bioresour. Technol. 2018;253:64-71.

[17] Gong X, Huang D, Liu Y, Zeng G, Wang R, Wan J, et al. Stabilized Nanoscale Zerovalent Iron Mediated Cadmium Accumulation and Oxidative Damage of Boehmeria nivea (L.) Gaudich Cultivated in Cadmium Contaminated Sediments. Environ. Sci. Technol. 2017;51(19):11308-16.

[18] Huang D, Deng R, Wan J, Zeng G, Xue W, Wen X, et al. Remediation of lead-contaminated sediment by biochar-supported nano-chlorapatite: Accompanied with the change of available phosphorus and organic matters. J. Hazard. Mater. 2018;348:109-16.

[19] Gong X, Huang D, Liu Y, Peng Z, Zeng G, Xu P, et al. Remediation of contaminated soils by biotechnology with nanomaterials: bio-behavior, applications, and perspectives. Crit. Rev. Biotechnol. 2018;38(3):455-68.

Accepted MS

[20] Hu C, Huang D, Zeng G, Cheng M, Gong X, Wang R, et al. The combination of Fenton process and Phanerochaete chrysosporium for the removal of bisphenol A in river sediments: Mechanism related to extracellular enzyme, organic acid and iron. Chem. Eng. J. 2018;338:432-9.

[21] Cheng M, Zeng G, Huang D, Lai C, Liu Y, Zhang C, et al. Efficient degradation of sulfamethazine in simulated and real wastewater at slightly basic pH values using Co-SAM-SCS/$H_2O_2$ Fenton-like system. Water Res. 2018:138:7-18.

[22] Cheng M, Zeng G, Huang D, Lai C, Liu Y, Xu P, et al. Salicylic acid–methanol modified steel converter slag as heterogeneous Fenton-like catalyst for enhanced degradation of alachlor. Chem. Eng. J. 2017;327:686-93.

[23] Deng J-H, Zhang X-R, Zeng G-M, Gong J-L, Niu Q-Y, Liang J. Simultaneous removal of Cd(II) and ionic dyes from aqueous solution using magnetic graphene oxide nanocomposite as an adsorbent. Chem. Eng. J. 2013;226:189-200.

[24] Long F, Gong J-L, Zeng G-M, Chen L, Wang X-Y, Deng J-H, et al. Removal of phosphate from aqueous solution by magnetic Fe-Zr binary oxide. Chem. Eng. J. 2011;171(2):448-55.

[25] Ren X, Zeng G, Tang L, Wang J, Wan J, Liu Y, et al. Sorption, transport and biodegradation - An insight into bioavailability of persistent organic pollutants in soil. Sci. Total Environ. 2018;610:1154-63.

[26] Zhang C, Lai C, Zeng G, Huang D, Tang L, Yang C, et al. Nanoporous Au-based chronocoulometric aptasensor for amplified detection of $Pb^{2+}$ using DNAzyme modified with Au nanoparticles. Biosens. Bioelectron. 2016;81:61-7.

Accepted MS

[27] Huang D, Li Z, Zeng G, Zhou C, Xue W, Gong X, et al. Megamerger in photocatalytic field: 2D g-$C_3N_4$ nanosheets serve as support of 0D nanomaterials for improving photocatalytic performance. Appl. Catal. B: Environ. 2019;240:153-73.

[28] Huang D, Wang X, Zhang C, Zeng G, Peng Z, Zhou J, et al. Sorptive removal of ionizable antibiotic sulfamethazine from aqueous solution by graphene oxide-coated biochar nanocomposites: Influencing factors and mechanism. Chemosphere. 2017;186:414-21.

[29] Wang R-Z, Huang D-L, Liu Y-G, Zhang C, Lai C, Zeng G-M, et al. Investigating the adsorption behavior and the relative distribution of $Cd^{2+}$ sorption mechanisms on biochars by different feedstock. Bioresour. Technol. 2018;261:265-71.

[30] Guo X, Peng Z, Huang D, Xu P, Zeng G, Zhou S, et al. Biotransformation of cadmium-sulfamethazine combined pollutant in aqueous environments: Phanerochaete chrysosporium using cautious optimism. Chem. Eng. J. 2018;347:74-83.

[31] Fang F, Rao S, Tang Z, Song P, Wang H. Improved flame resistance and thermo-mechanical properties of epoxy resin nanocomposites from functionalized graphene oxide via self-assembly in water. Compos B Eng. 2019;165:406-16.

[32] Wang H, Zeng Z, Xu P, Li L, Zeng G, Xiao R, et al. Recent progress in covalent organic framework thin films: fabrications, applications and perspectives. Chem. Soc. Rev. 2018;48:488-516.

[33] Lai C, Li B, Chen M, Zeng G, Huang D, Qin L, et al. Simultaneous degradation of P-nitroaniline and electricity generation by using a microfiltration membrane

Accepted MS

dual-chamber microbial fuel cell. Int. J. Hydrogen Energy 2018;43(3):1749-57.

[34] Xu P, Zeng GM, Huang DL, Lai C, Zhao MH, Wei Z, et al. Adsorption of Pb(II) by iron oxide nanoparticles immobilized Phanerochaete chrysosporium: Equilibrium, kinetic, thermodynamic and mechanisms analysis. Chem. Eng. J. 2012;203:423-31.

[35] Zhang Y, Zeng GM, Tang L, Chen J, Zhu Y, He XX, et al. Electrochemical Sensor Based on Electrodeposited Graphene-Au Modified Electrode and NanoAu Carrier Amplified Signal Strategy for Attomolar Mercury Detection. Anal. Chem. 2015;87(2):989-96.

[36] Huang D, Chen S, Zeng G, Gong X, Zhou C, Cheng M, et al. Artificial Z-scheme photocatalytic system: What have been done and where to go? Coord. Chem. Rev. 2019;385:44-80.

[37] Zhang J, Wang H, Yuan X, Zeng G, Tu W, Wang S. Tailored indium sulfide-based materials for solar-energy conversion and utilization. J. Photochem. Photobiol., C 2019;38:1-26.

[38] Li B, Lai C, Zeng G, Huang D, Qin L, Zhang M, et al. Black Phosphorus, a Rising Star 2D Nanomaterial in the Post-Graphene Era: Synthesis, Properties, Modifications, and Photocatalysis Applications. Small. 2019;15(8):e1804565.

[39] Tang N, Niu CG, Li XT, Liang C, Guo H, Lin LS, et al. Efficient removal of Cd(2+) and Pb(2+) from aqueous solution with amino- and thiol-functionalized activated carbon: Isotherm and kinetics modeling. Sci. Total Environ. 2018;635:1331-44.

[40] Mai Oanh LT, Hang LT, Lai ND, Phuong NT, Thang DV, Hung NM, et al.

Accepted MS

Influence of annealing temperature on physical properties and photocatalytic ability of g-$C_3N_4$ nanosheets synthesized through urea polymerization in Ar atmosphere. Physica B: Condensed Matter. 2018;532:48-53.

[41] Tang L, Deng Y, Zeng G, Hu W, Wang J, Zhou Y, et al. CdS/$Cu_2S$ co-sensitized $TiO_2$ branched nanorod arrays of enhanced photoelectrochemical properties by forming nanoscale heterostructure. J. Alloys Compd. 2016;662:516-27.

[42] Marien CBD, Cottineau T, Robert D, Drogui P. TiO2 Nanotube arrays: Influence of tube length on the photocatalytic degradation of Paraquat. Appl. Catal. B: Environ. 2016;194:1-6.

[43] Vaiano V, Matarangolo M, Murcia JJ, Rojas H, Navío JA, Hidalgo MC. Enhanced photocatalytic removal of phenol from aqueous solutions using ZnO modified with Ag. Appl. Catal. B: Environ. 2018;225:197-206.

[44] Zhang X, Zhang P, Wang L, Gao H, Zhao J, Liang C, et al. Template-oriented synthesis of monodispersed $SnS_2$@$SnO_2$ hetero-nanoflowers for Cr(VI) photoreduction. Appl. Catal. B: Environ. 2016;192:17-25.

[45] Jiang L, Yuan X, Zeng G, Liang J, Chen X, Yu H, et al. In-situ synthesis of direct solid-state dual Z-scheme $WO_3$/g-$C_3N_4$/$Bi_2O_3$ photocatalyst for the degradation of refractory pollutant. Appl. Catal. B: Environ. 2018;227:376-85.

[46] Jiang L, Yuan X, Zeng G, Wu Z, Liang J, Chen X, et al. Metal-free efficient photocatalyst for stable visible-light photocatalytic degradation of refractory pollutant. Appl. Catal. B: Environ. 2018;221:715-25.

[47] Liu C, Zhang Y, Dong F, Reshak AH, Ye L, Pinna N, et al. Chlorine intercalation

Accepted MS

in graphitic carbon nitride for efficient photocatalysis. Appl. Catal. B: Environ. 2017;203:465-74.

[48] Hu S, Li F, Fan Z, Wang F, Zhao Y, Lv Z. Band gap-tunable potassium doped graphitic carbon nitride with enhanced mineralization ability. Dalton Trans. 2015;44(3):1084-92.

[49] Zhou C, Lai C, Huang D, Zeng G, Zhang C, Cheng M, et al. Highly porous carbon nitride by supramolecular preassembly of monomers for photocatalytic removal of sulfamethazine under visible light driven. Appl. Catal. B: Environ. 2018;220:202-10.

[50] Huang H, Xiao K, Tian N, Dong F, Zhang T, Du X, et al. Template-free precursor-surface-etching route to porous, thin g-$C_3N_4$ nanosheets for enhancing photocatalytic reduction and oxidation activity. J. Mater. Chem. A. 2017;5(33):17452-63.

[51] Pakdel A, Bando Y, Golberg D. Nano boron nitride flatland. Chem. Soc. Rev. 2014;43(3):934-59.

[52] Zhi C, Bando Y, Tang C, Golberg D. Boron nitride nanotubes. Materials Science and Engineering: R: Reports. 2010;70(3-6):92-111.

[53] Ansari SA, Khan MM, Kalathil S, Nisar A, Lee J, Cho MH. Oxygen vacancy induced band gap narrowing of ZnO nanostructures by an electrochemically active biofilm. Nanoscale. 2013;5(19):9238-46.

[54] Khan MM, Ansari SA, Pradhan D, Ansari MO, Han DH, Lee J, et al. Band gap engineered $TiO_2$ nanoparticles for visible light induced photoelectrochemical and

Accepted MS

photocatalytic studies. J Mater Chem A. 2014;2(3):637-44.

[55] Sharma K, Maiti K, Kim NH, Hui D, Lee JH. Green synthesis of glucose-reduced graphene oxide supported Ag-$Cu_2O$ nanocomposites for the enhanced visible-light photocatalytic activity. Compos B Eng. 2018;138:35-44.

[56] Ojha DP, Karki HP, Song JH, Kim HJ. Amine-assisted synthesis of $FeWO_4$ nanorod g-$C_3N_4$ for enhanced visible light-driven Z-scheme photocatalysis. Compos B Eng. 2019;160:277-84.

[57] Ghafari E, Feng Y, Liu Y, Ferguson I, Lu N. Investigating process-structure relations of ZnO nanofiber via electrospinning method. Compos B Eng. 2017;116:40-5.

[58] Dong H, Zeng G, Tang L, Fan C, Zhang C, He X, et al. An overview on limitations of $TiO_2$-based particles for photocatalytic degradation of organic pollutants and the corresponding countermeasures. Water Res. 2015;79:128-46.

[59] Martins PM, Ferreira CG, Silva AR, Magalhães B, Alves MM, Pereira L, et al. $TiO_2$/graphene and $TiO_2$/graphene oxide nanocomposites for photocatalytic applications: A computer modeling and experimental study. Compos B Eng. 2018;145:39-46.

[60] Dai J, Tian Q, Sun Q, Wei W, Zhuang J, Liu M, et al. $TiO_2$-alginate composite aerogels as novel oil/water separation and wastewater remediation filters. Compos B Eng. 2019;160:480-7.

[61] Wang W, Tadé MO, Shao Z. Nitrogen-doped simple and complex oxides for photocatalysis: A review. Prog. Mater Sci. 2018;92:33-63.

Accepted MS

[62] Asahi R, Morikawa T, Ohwaki T, Aoki K, Taga Y. Visible-light photocatalysis in nitrogen-doped titanium oxides. science. 2001;293(5528):269-71.

[63] Chen X, Burda C. The electronic origin of the visible-light absorption properties of C-, N-and S-doped $TiO_2$ nanomaterials. J. Am. Chem. Soc. 2008;130(15):5018-9.

[64] Ansari SA, Khan MM, Ansari MO, Cho MH. Nitrogen-doped titanium dioxide (N-doped $TiO_2$) for visible light photocatalysis. New J. Chem.2016;40(4):3000-9.

[65] Boningari T, Inturi SNR, Suidan M, Smirniotis PG. Novel one-step synthesis of nitrogen-doped $TiO_2$ by flame aerosol technique for visible-light photocatalysis: Effect of synthesis parameters and secondary nitrogen (N) source. Chem. Eng. J. 2018;350:324-34.

[66] Asahi R, Morikawa T, Irie H, Ohwaki T. Nitrogen-Doped Titanium Dioxide as Visible-Light-Sensitive Photocatalyst: Designs, Developments, and Prospects. Chem. Rev. 2014;114(19):9824-52.

[67] Jiang L, Yuan X, Pan Y, Liang J, Zeng G, Wu Z, et al. Doping of graphitic carbon nitride for photocatalysis: A reveiw. Appl. Catal. B: Environ. 2017;217:388-406.

[68] Zhao Z, Sun Y, Dong F. Graphitic carbon nitride based nanocomposites: a review. Nanoscale. 2015;7(1):15-37.

[69] Mamba G, Mishra AK. Graphitic carbon nitride (g-$C_3N_4$) nanocomposites: A new and exciting generation of visible light driven photocatalysts for environmental pollution remediation. Appl. Catal. B: Environ. 2016;198:347-77.

[70] Chowdhury S, Balasubramanian R. Graphene/semiconductor nanocomposites (GSNs) for heterogeneous photocatalytic decolorization of wastewaters contaminated

Accepted MS

with synthetic dyes: A review. Appl. Catal. B: Environ. 2014;160-161:307-24.

[71] Ng YH, Ikeda S, Matsumura M, Amal R. A perspective on fabricating carbon-based nanomaterials by photocatalysis and their applications. Energy Environ. Sci. 2012;5(11):9307.

[72] Perathoner S, Ampelli C, Chen S, Passalacqua R, Su D, Centi G. Photoactive materials based on semiconducting nanocarbons – A challenge opening new possibilities for photocatalysis. J. Energy Chem. 2017;26(2):207-18.

[73] Sakaushi K, Antonietti M. Carbon- and Nitrogen-Based Porous Solids: A Recently Emerging Class of Materials. Bull. Chem. Soc. Jpn. 2015;88(3):386-98.

[74] Scida K, Stege PW, Haby G, Messina GA, Garcia CD. Recent applications of carbon-based nanomaterials in analytical chemistry: critical review. Anal. Chim. Acta 2011;691(1-2):6-17.

[75] Liu S, Chevali VS, Xu Z, Hui D, Wang H. A review of extending performance of epoxy resins using carbon nanomaterials. Compos B Eng. 2018;136:197-214.

[76] Song B, Xu P, Zeng G, Gong J, Zhang P, Feng H, et al. Carbon nanotube-based environmental technologies: the adopted properties, primary mechanisms, and challenges. Rev. Environ. Sci. Bio. 2018;17(3):571-90.

[77] Elishav O, Lewin DR, Shter GE, Grader GS. The nitrogen economy: Economic feasibility analysis of nitrogen-based fuels as energy carriers. Appl. Energy 2017;185:183-8.

[78] Masih D, Ma Y, Rohani S. Graphitic $C_3N_4$ based noble-metal-free photocatalyst systems: A review. Appl. Catal. B: Environ. 2017;206:556-88.

Accepted MS

[79] Hu C, Chu Y-C, Wang M-S, Wu X-H. Rapid synthesis of g-$C_3N_4$ spheres using microwave-assisted solvothermal method for enhanced photocatalytic activity. J. Photochem. Photobiol., A 2017;348:8-17.

[80] Cui Y, Ding Z, Fu X, Wang X. Construction of conjugated carbon nitride nanoarchitectures in solution at low temperatures for photoredox catalysis. Angewandte Chemie. 2012;51(47):11814-8.

[81] Cao C, Huang F, Cao C, Li J, Zhu H. Synthesis of carbon nitride nanotubes via a catalytic-assembly solvothermal route. Chem. Mater. 2004;16(25):5213-5.

[82] Li J, Cao C, Hao J, Qiu H, Xu Y, Zhu H. Self-assembled one-dimensional carbon nitride architectures. Diamond Relat. Mater. 2006;15(10):1593-600.

[83] Li Y, Zhang J, Wang Q, Jin Y, Huang D, Cui Q, et al. Nitrogen-rich carbon nitride hollow vessels: synthesis, characterizations, and their properties. The Journal of Physical Chemistry B. 2010;114(29):9429-34.

[84] Zimmerman JL, Williams R, Khabashesku VN, Margrave JL. Synthesis of spherical carbon nitride nanostructures. Nano Lett. 2001;1(12):731-4.

[85] Ma T, Bai J, Li C. Facile synthesis of g-$C_3N_4$ wrapping on one-dimensional carbon fiber as a composite photocatalyst to degrade organic pollutants. Vacuum. 2017;145:47-54.

[86] Wang L, Wang C, Hu X, Xue H, Pang H. Metal/Graphitic Carbon Nitride Composites: Synthesis, Structures, and Applications. Chemistry, an Asian journal. 2016;11(23):3305-28.

[87] Li C, Cao C-B, Zhu H-S. Graphitic carbon nitride thin films deposited by

Accepted MS

electrodeposition. Mater. Lett. 2004;58(12-13):1903-6.

[88] Li C, Cao C-B, Zhu H-S, Lv Q, Zhang J-T, Xiang X. Electrodeposition route to prepare graphite-like carbon nitride. Mater. Sci. Eng., B 2004;106(3):308-12.

[89] Bai X, Li J, Cao C. Synthesis of hollow carbon nitride microspheres by an electrodeposition method. Appl. Surf. Sci. 2010;256(8):2327-31.

[90] Shi H, Chen G, Zhang C, Zou Z. Polymeric g-$C_3N_4$ Coupled with $NaNbO_3$ Nanowires toward Enhanced Photocatalytic Reduction of $CO_2$ into Renewable Fuel. ACS Catal. 2014;4(10):3637-43.

[91] Wang Y, Wang X, Antonietti M. Polymeric graphitic carbon nitride as a heterogeneous organocatalyst: from photochemistry to multipurpose catalysis to sustainable chemistry. Angewandte Chemie International Edition. 2012;51(1):68-89.

[92] Lyth SM, Nabae Y, Moriya S, Kuroki S, Kakimoto M-a, Ozaki J-i, et al. Carbon nitride as a nonprecious catalyst for electrochemical oxygen reduction. J. Phys. Chem. C. 2009;113(47):20148-51.

[93] Xu CQ, Li K, Zhang WD. Enhancing visible light photocatalytic activity of nitrogen-deficient g-$C_3N_4$ via thermal polymerization of acetic acid-treated melamine. J. Colloid Interface Sci. 2017;495:27-36.

[94] Zhao Z, Ma Y, Fan J, Xue Y, Chang H, Masubuchi Y, et al. Synthesis of graphitic carbon nitride from different precursors by fractional thermal polymerization method and their visible light induced photocatalytic activities. J. Alloys Compd. 2018;735:1297-305.

[95] Xu M, Liang T, Shi M, Chen H. Graphene-like two-dimensional materials. Chem.

Accepted MS

Rev. 2013;113(5):3766-98.

[96] Yu S, Wang X, Pang H, Zhang R, Song W, Fu D, et al. Boron nitride-based materials for the removal of pollutants from aqueous solutions: A review. Chem. Eng. J. 2018;333:343-60.

[97] Novoselov KS, Geim AK, Morozov SV, Jiang D, Zhang Y, Dubonos SV, et al. Electric field effect in atomically thin carbon films. science. 2004;306(5696):666-9.

[98] Pacilé D, Meyer JC, Girit ÇÖ, Zettl A. The two-dimensional phase of boron nitride: Few-atomic-layer sheets and suspended membranes. Appl. Phys. Lett. 2008;92(13):133107.

[99] Li LH, Chen Y, Behan G, Zhang H, Petravic M, Glushenkov AM. Large-scale mechanical peeling of boron nitride nanosheets by low-energy ball milling. J. Mater. Chem. 2011;21(32):11862.

[100] Lin Y, Williams TV, Cao W, Elsayed-Ali HE, Connell JW. Defect functionalization of hexagonal boron nitride nanosheets. J. Phys. Chem. C. 2010;114(41):17234-9.

[101] Xu M, Fujita D, Sagisaka K, Watanabe E, Hanagata N. Production of extended single-layer graphene. ACS nano. 2011;5(2):1522-8.

[102] Song L, Ci L, Lu H, Sorokin PB, Jin C, Ni J, et al. Large scale growth and characterization of atomic hexagonal boron nitride layers. Nano lett. 2010;10(8):3209-15.

[103] Lourie OR, Jones CR, Bartlett BM, Gibbons PC, Ruoff RS, Buhro WE. CVD growth of boron nitride nanotubes. Chem. Mater. 2000;12(7):1808-10.

Accepted MS

[104] Gao R, Yin L, Wang C, Qi Y, Lun N, Zhang L, et al. High-yield synthesis of boron nitride nanosheets with strong ultraviolet cathodoluminescence emission. J. Phys. Chem. C. 2009;113(34):15160-5.

[105] Pierson HO. Boron nitride composites by chemical vapor deposition.J. Compos. Mater.1975;9(3):228-40.

[106] Rozenberg A, Sinenko YA, Chukanov N. Regularities of pyrolytic boron nitride coating formation on a graphite matrix. J. Mater. Sci.1993;28(20):5528-33.

[107] Middleman S. The role of gas-phase reactions in boron nitride growth by chemical vapor deposition. Mater. Sci. Eng., A1993;163(1):135-40.

[108] Adams A. Characterization of films formed by pyrolysis of borazine. J. Electrochem. Soc. 1981;128(6):1378-9.

[109] Constant G, Feurer R. Preparation and characterization of thin protective films in silica tubes by thermal decomposition of hexachloroborazine. Journal of the Less Common Metals. 1981;82:113-8.

[110] Müller F, Stöwe K, Sachdev H. Symmetry versus commensurability: Epitaxial growth of hexagonal boron nitride on Pt (111) from B-trichloroborazine (ClBNH)3. Chem. Mater. 2005;17(13):3464-7.

[111] Shi Y, Hamsen C, Jia X, Kim KK, Reina A, Hofmann M, et al. Synthesis of few-layer hexagonal boron nitride thin film by chemical vapor deposition. Nano lett. 2010;10(10):4134-9.

[112] Han W-Q, Wu L, Zhu Y, Watanabe K, Taniguchi T. Structure of chemically derived mono- and few-atomic-layer boron nitride sheets. Appl. Phys. Lett.

Accepted MS

2008;93(22):223103.

[113] Nag A, Raidongia K, Hembram KP, Datta R, Waghmare UV, Rao C. Graphene analogues of BN: novel synthesis and properties. ACS nano. 2010;4(3):1539-44.

[114] Lin Y, Williams TV, Xu T-B, Cao W, Elsayed-Ali HE, Connell JW. Aqueous Dispersions of Few-Layered and Monolayered Hexagonal Boron Nitride Nanosheets from Sonication-Assisted Hydrolysis: Critical Role of Water. J. Phys. Chem. C. 2011;115(6):2679-85.

[115] Zhang K, Feng Y, Wang F, Yang Z, Wang J. Two dimensional hexagonal boron nitride (2D-hBN): synthesis, properties and applications. J. Mater. Chem. C. 2017;5(46):11992-2022.

[116] Zeng G, Wan J, Huang D, Hu L, Huang C, Cheng M, et al. Precipitation, adsorption and rhizosphere effect: The mechanisms for Phosphate-induced Pb immobilization in soils—A review. J. Hazard. Mater. 2017;339:354-67.

[117] Hu L, Wan J, Zeng G, Chen A, Chen G, Huang Z, et al. Comprehensive evaluation of the cytotoxicity of CdSe/ZnS quantum dots in Phanerochaete chrysosporium by cellular uptake and oxidative stress. Environ. Sci. Nano. 2017;4(10):2018-29.

[118] Li H, Wang L, Liu Y, Lei J, Zhang J. Mesoporous graphitic carbon nitride materials: synthesis and modifications. Res. Chem. Intermed.2015;42(5):3979-98.

[119] Zhang G, Zhang J, Zhang M, Wang X. Polycondensation of thiourea into carbon nitride semiconductors as visible light photocatalysts. J. Mater. Chem. 2012;22(16):8083.

Accepted MS

[120] Akhmedov VM, Melnikova NE, Akhmedov ID. Synthesis, properties, and application of polymeric carbon nitrides. Russ. Chem. Bull.2017;66(5):782-807.

[121] Li Y, Sun Y, Ho W, Zhang Y, Huang H, Cai Q, et al. Highly enhanced visible-light photocatalytic NOx purification and conversion pathway on self-structurally modified g-C3N4 nanosheets. Sci. Bull. 2018;63(10):609-20.

[122] Chen P, Dong F, Ran M, Li J. Synergistic photo-thermal catalytic NO purification of $MnO_x$/g-$C_3N_4$: Enhanced performance and reaction mechanism. Chin. J. Catal. 2018;39(4):619-29.

[123] Wang H, He W, Dong Xa, Wang H, Dong F. In situ FT-IR investigation on the reaction mechanism of visible light photocatalytic NO oxidation with defective g-$C_3N_4$. Sci. Bull. 2018;63(2):117-25.

[124] Patnaik S, Martha S, Parida KM. An overview of the structural, textural and morphological modulations of g-$C_3N_4$ towards photocatalytic hydrogen production. RSC Adv. 2016;6(52):46929-51.

[125] Xu J, Zhang L, Shi R, Zhu Y. Chemical exfoliation of graphitic carbon nitride for efficient heterogeneous photocatalysis. J. Mater. Chem. A. 2013;1(46):14766.

[126] Wen J, Xie J, Chen X, Li X. A review on g-$C_3N_4$-based photocatalysts. Appl. Surf. Sci. 2017;391:72-123.

[127] Darkwah WK, Ao Y. Mini Review on the Structure and Properties (Photocatalysis), and Preparation Techniques of Graphitic Carbon Nitride Nano-Based Particle, and Its Applications. Nanoscale Res. Lett. 2018;13(1):388.

[128] Zhang C, Li Y, Shuai D, Shen Y, Xiong W, Wang L. Graphitic carbon nitride

Accepted MS

($g\text{-}C_3N_4$)-based photocatalysts for water disinfection and microbial control: A review. Chemosphere. 2019;214:462-79.

[129] Barrio J, Shalom M. Rational Design of Carbon Nitride Materials by Supramolecular Preorganization of Monomers. ChemCatChem. 2018;10(24):5573-86.

[130] Ye S, Yan M, Tan X, Liang J, Zeng G, Wu H, et al. Facile assembled biochar-based nanocomposite with improved graphitization for efficient photocatalytic activity driven by visible light. Appl. Catal. B: Environ. 2019;250:78-88.

[131] Fu J, Yu J, Jiang C, Cheng B. $g\text{-}C_3N_4$-Based Heterostructured Photocatalysts. Adv. Energy Mater. 2018;8(3):1701503.

[132] Fu Y, Xu P, Huang D, Zeng G, Lai C, Qin L, et al. Au nanoparticles decorated on activated coke via a facile preparation for efficient catalytic reduction of nitrophenols and azo dyes. Appl. Surf. Sci. 2019;473:578-88.

[133] Nikokavoura A, Trapalis C. Graphene and $g\text{-}C_3N_4$ based photocatalysts for NO x removal: A review. Appl. Surf. Sci. 2018;430:18-52.

[134] Patnaik S, Sahoo DP, Parida K. An overview on Ag modified $g\text{-}C_3N_4$ based nanostructured materials for energy and environmental applications. Renewable Sustainable Energy Rev. 2018;82:1297-312.

[135] Lam S-M, Sin J-C, Mohamed AR. A review on photocatalytic application of $g\text{-}C_3N_4$/semiconductor (CNS) nanocomposites towards the erasure of dyeing wastewater. Mater. Sci. Semicond. Process. 2016;47:62-84.

[136] Yi H, Yan M, Huang D, Zeng G, Lai C, Li M, et al. Synergistic effect of

Accepted MS

artificial enzyme and 2D nano-structured $Bi_2WO_6$ for eco-friendly and efficient biomimetic photocatalysis. Appl. Catal. B: Environ. 2019;250:52-62.

[137] Yi H, Qin L, Huang D, Zeng G, Lai C, Liu X, et al. Nano-structured bismuth tungstate with controlled morphology: Fabrication, modification, environmental application and mechanism insight. Chem. Eng. J. 2019;358:480-96.

[138] Bi L, Xu D, Zhang L, Lin Y, Wang D, Xie T. Metal Ni-loaded g-$C_3N_4$ for enhanced photocatalytic $H_2$ evolution activity: the change in surface band bending. Physical chemistry chemical physics : PCCP. 2015;17(44):29899-905.

[139] Patnaik S, Martha S, Acharya S, Parida KM. An overview of the modification of g-$C_3N_4$ with high carbon containing materials for photocatalytic applications. Inorganic Chemistry Frontiers. 2016;3(3):336-47.

[140] Yin S, Han J, Zhou T, Xu R. Recent progress in g-$C_3N_4$ based low cost photocatalytic system: activity enhancement and emerging applications. Catal. Sci. Technol. 2015;5(12):5048-61.

[141] Fu X, Hu Y, Yang Y, Liu W, Chen S. Ball milled h-BN: an efficient holes transfer promoter to enhance the photocatalytic performance of $TiO_2$. J. Hazard. Mater. 2013;244-245:102-10.

[142] Fu X, Hu Y, Zhang T, Chen S. The role of ball milled h-BN in the enhanced photocatalytic activity: A study based on the model of ZnO. Appl. Surf. Sci. 2013;280:828-35.

[143] Zhou C, Lai C, Zhang C, Zeng G, Huang D, Cheng M, et al. Semiconductor/boron nitride composites: Synthesis, properties, and photocatalysis

Accepted MS

applications. Appl. Catal. B: Environ. 2018;238:6-18.

[144] Watanabe K, Taniguchi T, Kanda H. Direct-bandgap properties and evidence for ultraviolet lasing of hexagonal boron nitride single crystal. Nat. Mater. 2004;3(6):404-9.

[145] Yu J, Qin L, Hao Y, Kuang S, Bai X, Chong Y-M, et al. Vertically aligned boron nitride nanosheets: chemical vapor synthesis, ultraviolet light emission, and superhydrophobicity. ACS nano. 2010;4(1):414-22.

[146] Pakdel A, Zhi C, Bando Y, Nakayama T, Golberg D. Boron nitride nanosheet coatings with controllable water repellency. ACS Nano. 2011;5(8):6507-15.

[147] Gorbachev RV, Riaz I, Nair RR, Jalil R, Britnell L, Belle BD, et al. Hunting for monolayer boron nitride: optical and Raman signatures. Small. 2011;7(4):465-8.

[148] Pakdel A, Wang X, Zhi C, Bando Y, Watanabe K, Sekiguchi T, et al. Facile synthesis of vertically aligned hexagonal boron nitride nanosheets hybridized with graphitic domains. J. Mater. Chem. 2012;22(11):4818.

[149] Ci L, Song L, Jin C, Jariwala D, Wu D, Li Y, et al. Atomic layers of hybridized boron nitride and graphene domains. Nat. Mater. 2010;9(5):430-5.

[150] Qin L, Yu J, Kuang S, Xiao C, Bai X. Few-atomic-layered boron carbonitride nanosheets prepared by chemical vapor deposition. Nanoscale. 2012;4(1):120-3.

[151] Samokhvalov A. Hydrogen by photocatalysis with nitrogen codoped titanium dioxide. Renewable Sustainable Energy Rev. 2017;72:981-1000.

[152] Pablos C, Marugan J, van Grieken R, Dunlop PSM, Hamilton JWJ, Dionysiou DD, et al. Electrochemical Enhancement of Photocatalytic Disinfection on Aligned

Accepted MS

TiO(2) and Nitrogen Doped TiO(2) Nanotubes. Molecules. 2017;22(5).

[153] Keraudy J, Ferrec A, Richard-Plouet M, Hamon J, Goullet A, Jouan P-Y. Nitrogen doping on NiO by reactive magnetron sputtering: A new pathway to dynamically tune the optical and electrical properties. Appl. Surf. Sci. 2017;409:77-84.

[154] Wan JX, You Y, Xu YL, Wang C, Zhang PB, Jiang XY, et al. Synthesis of nitrogen-doped graphene via pentachloropyridine as the sole solid source. Appl. Phys. Lett. 2017;111(3):033106.

[155] NARAYANAN N, DEEPAK NK. IMPACT OF N DOPING ON THE PHYSICAL PROPERTIES OF ZnO THIN FILMS. Surf. Rev. Lett. 2018;25(01):1850035.

[156] Oliveira JA, Nogueira AE, Gonçalves MCP, Paris EC, Ribeiro C, Poirier GY, et al. Photoactivity of N-doped ZnO nanoparticles in oxidative and reductive reactions. Appl. Surf. Sci. 2018;433:879-86.

[157] Kumar S, Reddy NL, Kumar A, Shankar MV, Krishnan V. Two dimensional N-doped ZnO-graphitic carbon nitride nanosheets heterojunctions with enhanced photocatalytic hydrogen evolution. Int. J. Hydrogen Energy 2018;43(8):3988-4002.

[158] Chen M, Huang Y, Yao J, Cao J-j, Liu Y. Visible-light-driven N-$(BiO)_2CO_3$ /Graphene oxide composites with improved photocatalytic activity and selectivity for NO x removal. Appl. Surf. Sci. 2018;430:137-44.

[159] Dong F, Sun Y, Fu M, Ho WK, Lee SC, Wu Z. Novel in situ N-doped $(BiO)_2CO_3$ hierarchical microspheres self-assembled by nanosheets as efficient and

Accepted MS

durable visible light driven photocatalyst. Langmuir : the ACS journal of surfaces and colloids. 2012;28(1):766-73.

[160] Dong F, Liu H, Ho W-K, Fu M, Wu Z. (NH4)2CO3 mediated hydrothermal synthesis of N-doped $(BiO)_2CO_3$ hollow nanoplates microspheres as high-performance and durable visible light photocatalyst for air cleaning. Chem. Eng. J. 2013;214:198-207.

[161] Xiong T, Dong Xa, Huang H, Cen W, Zhang Y, Dong F. Single Precursor Mediated-Synthesis of Bi Semimetal Deposited N-Doped $(BiO)_2CO_3$ Superstructures for Highly Promoted Photocatalysis. ACS Sustain. Chem. Eng. 2016;4(6):2969-79.

[162] Osterloh FE. Inorganic nanostructures for photoelectrochemical and photocatalytic water splitting. Chem. Soc. Rev. 2013;42(6):2294-320.

[163] Zou X, Zhang Y. Noble metal-free hydrogen evolution catalysts for water splitting. Chem. Soc. Rev. 2015;44(15):5148-80.

[164] Wang X, Maeda K, Thomas A, Takanabe K, Xin G, Carlsson JM, et al. A metal-free polymeric photocatalyst for hydrogen production from water under visible light. Nat. mater. 2009;8(1):76-80.

[165] Wang X, Maeda K, Chen X, Takanabe K, Domen K, Hou Y, et al. Polymer semiconductors for artificial photosynthesis: hydrogen evolution by mesoporous graphitic carbon nitride with visible light. J. Am. Chem. Soc. 2009;131(5):1680-1.

[166] Zhang J, Guo F, Wang X. An optimized and general synthetic strategy for fabrication of polymeric carbon nitride nanoarchitectures. Adv. Funct. Mater. 2013;23(23):3008-14.

Accepted MS

[167] Zhao S, Zhang Y, Zhou Y, Wang Y, Qiu K, Zhang C, et al. Facile one-step synthesis of hollow mesoporous g-$C_3N_4$ spheres with ultrathin nanosheets for photoredox water splitting. Carbon. 2018;126:247-56.

[168] Niu P, Zhang L, Liu G, Cheng H-M. Graphene-Like Carbon Nitride Nanosheets for Improved Photocatalytic Activities. Adva. Funct. Mater. 2012;22(22):4763-70.

[169] Chen F, Yang Q, Wang Y, Zhao J, Wang D, Li X, et al. Novel ternary heterojunction photcocatalyst of Ag nanoparticles and g-$C_3N_4$ nanosheets co-modified $BiVO_4$ for wider spectrum visible-light photocatalytic degradation of refractory pollutant. Appl. Catal. B: Environ. 2017;205:133-47.

[170] Guo H, Niu C-G, Zhang L, Wen X-J, Liang C, Zhang X-G, et al. Construction of Direct Z-Scheme AgI/$Bi_2Sn_2O_7$ Nanojunction System with Enhanced Photocatalytic Activity: Accelerated Interfacial Charge Transfer Induced Efficient Cr(VI) Reduction, Tetracycline Degradation and Escherichia coli Inactivation. ACS Sustain. Chem. Eng. 2018;6(6):8003-18.

[171] Guo H, Niu CG, Wen XJ, Zhang L, Liang C, Zhang XG, et al. Construction of highly efficient and stable ternary AgBr/Ag/$PbBiO_2Br$ Z-scheme photocatalyst under visible light irradiation: Performance and mechanism insight. J. Colloid Interface Sci. 2018;513:852-65.

[172] Tian N, Zhang Y, Li X, Xiao K, Du X, Dong F, et al. Precursor-reforming protocol to 3D mesoporous g-$C_3N_4$ established by ultrathin self-doped nanosheets for superior hydrogen evolution. Nano Energy. 2017;38:72-81.

[173] Zhou Y, Zhang L, Huang W, Kong Q, Fan X, Wang M, et al. N-doped graphitic

Accepted MS

carbon-incorporated g-$C_3N_4$ for remarkably enhanced photocatalytic $H_2$ evolution under visible light. Carbon. 2016;99:111-7.

[174] Cheng J, Hu X, Zhang J, Huang H, Su N, Zhu H. Fabrication of a composite of platinum, N-g-$C_3N_4$ and Ketjen Black for photo-electrochemical methanol oxidation. J. Mater. Sci. 2017;52(14):8444-54.

[175] Weng Q, Wang X, Wang X, Bando Y, Golberg D. Functionalized hexagonal boron nitride nanomaterials: emerging properties and applications. Chem. Soc. Rev. 2016;45(14):3989-4012.

[176] Fang Y, Wang X. Metal‐Free Boron‐Containing Heterogeneous Catalysts. Angewandte Chemie International Edition. 2017;56(49):15506-18.

[177] Lin T, Huang F, Liang J, Wang Y. A facile preparation route for boron-doped graphene, and its CdTe solar cell application. Energy Environ Sci. 2011;4(3):862-5.

[178] Chen L, Wang X. Bio-templated fabrication of metal-free boron carbonitride tubes for visible light photocatalysis. Chem. Commun. 2017;53(88):11988-91.

[179] Huang C, Chen C, Zhang M, Lin L, Ye X, Lin S, et al. Carbon-doped BN nanosheets for metal-free photoredox catalysis. Nature communications. 2015;6:7698.

[180] Fujishima A, Honda K. Electrochemical photolysis of water at a semiconductor electrode. nature. 1972;238(5358):37.

[181] Reddy PAK, Reddy PVL, Kim K-H, Kumar MK, Manvitha C, Shim J-J. Novel approach for the synthesis of nitrogen-doped titania with variable phase composition and enhanced production of hydrogen under solar irradiation. J. Ind. Eng. Chem. 2017;53:253-60.

Accepted MS

[182] Shi R, Li Z, Yu H, Shang L, Zhou C, Waterhouse GIN, et al. Effect of Nitrogen Doping Level on the Performance of N-Doped Carbon Quantum Dot/$TiO_2$ Composites for Photocatalytic Hydrogen Evolution. ChemSusChem. 2017;10(22):4650-6.

[183] Yu H, Shi R, Zhao Y, Waterhouse GI, Wu LZ, Tung CH, et al. Smart Utilization of Carbon Dots in Semiconductor Photocatalysis. Adv. Mater. 2016;28(43):9454-77.

[184] Jing S, Zhang L, Luo L, Lu J, Yin S, Shen PK, et al. N-Doped Porous Molybdenum Carbide Nanobelts as Efficient Catalysts for Hydrogen Evolution Reaction. Appl. Catal. B: Environ. 2018;224:533-40.

[185] Lai L, Potts JR, Zhan D, Wang L, Poh CK, Tang C, et al. Exploration of the active center structure of nitrogen-doped graphene-based catalysts for oxygen reduction reaction. Energy Environ. Sci. 2012;5(7):7936.

[186] Liu Y, Yu G, Li GD, Sun Y, Asefa T, Chen W, et al. Coupling $Mo_2C$ with Nitrogen-Rich Nanocarbon Leads to Efficient Hydrogen-Evolution Electrocatalytic Sites. Angewandte Chemie. 2015;54(37):10752-7.

[187] Zhang C, Liu Y, Zeng G-M, Huang D-L, Lai C, Huang C, et al. Utilization of nano-gold tracing technique: study the adsorption and transmission of laccase in mediator-involved enzymatic degradation of lignin during solid-state fermentation. BioChem. Eng. J. 2014;91:149-56.

[188] Zhang C, Zeng G, Huang D, Lai C, Huang C, Li N, et al. Combined removal of di (2-ethylhexyl) phthalate (DEHP) and Pb (II) by using a cutinase loaded nanoporous gold-polyethyleneimine adsorbent. RSC Adv. 2014;4(98):55511-8.

Accepted MS

[189] Wu H, Lai C, Zeng G, Liang J, Chen J, Xu J, et al. The interactions of composting and biochar and their implications for soil amendment and pollution remediation: a review. Crit. Rev. Biotechnol. 2017;37(6):754-64.

[190] Yang Y, Zhang C, Lai C, Zeng G, Huang D, Cheng M, et al. BiOX (X = Cl, Br, I) photocatalytic nanomaterials: Applications for fuels and environmental management. Adv. Colloid Interface Sci. 2018;254:76-93.

[191] Chen M, Qin X, Zeng G. Biodegradation of Carbon Nanotubes, Graphene, and Their Derivatives. Trends Biotechnol. 2017;35(9):836-46.

[192] Chen M, Zeng G, Xu P, Yan M, Xiong W, Zhou S. Interaction of carbon nanotubes with microbial enzymes: conformational transitions and potential toxicity. Environ. Sci. Nano. 2017;4(10):1954-60.

[193] Chen M, Zeng G, Xu P, Zhang Y, Jiang D, Zhou S. Understanding enzymatic degradation of single-walled carbon nanotubes triggered by functionalization using molecular dynamics simulation. Environ. Sci. Nano. 2017;4(3):720-7.

[194] Huang D, Guo X, Peng Z, Zeng G, Xu P, Gong X, et al. White rot fungi and advanced combined biotechnology with nanomaterials: promising tools for endocrine-disrupting compounds biotransformation. Crit. Rev. Biotechnol. 2017:1-19.

[195] Zhang C, Wang W, Duan A, Zeng G, Huang D, Lai C, et al. Adsorption behavior of engineered carbons and carbon nanomaterials for metal endocrine disruptors: Experiments and theoretical calculation. Chemosphere. 2019;222:184-94.

[196] Liu Y, Liu Z, Huang D, Cheng M, Zeng G, Lai C, et al. Metal or metal-containing nanoparticle@MOF nanocomposites as a promising type of

Accepted MS

photocatalyst. Coord. Chem. Rev. 2019;388:63-78.

[197] Zhang C, Lai C, Zeng G, Huang D, Yang C, Wang Y, et al. Efficacy of carbonaceous nanocomposites for sorbing ionizable antibiotic sulfamethazine from aqueous solution. Water Res. 2016;95:103-12.

[198] Zeng G, Zhang C, Huang D, Lai C, Tang L, Zhou Y, et al. Practical and regenerable electrochemical aptasensor based on nanoporous gold and thymine-$Hg^{2+}$-thymine base pairs for $Hg^{2+}$ detection. Biosens. Bioelectron. 2017;90:542-8.

[199] Wang W, Xu P, Chen M, Zeng G, Zhang C, Zhou C, et al. Alkali Metal-Assisted Synthesis of Graphite Carbon Nitride with Tunable Band-Gap for Enhanced Visible-Light-Driven Photocatalytic Performance. ACS Sustain. Chem. Eng. 2018;6(11):15503-16.

[200] Xiong W, Zeng Z, Li X, Zeng G, Xiao R, Yang Z, et al. Multi-walled carbon nanotube/amino-functionalized MIL-53(Fe) composites: Remarkable adsorptive removal of antibiotics from aqueous solutions. Chemosphere. 2018;210:1061-9.

[201] Yang J, Liu X, Wang D, Xu Q, Yang Q, Zeng G, et al. Mechanisms of peroxymonosulfate pretreatment enhancing production of short-chain fatty acids from waste activated sludge. Water Res. 2019;148:239-49.

[202] Ong WJ, Tan LL, Ng YH, Yong ST, Chai SP. Graphitic Carbon Nitride ($g\text{-}C_3N_4$)-Based Photocatalysts for Artificial Photosynthesis and Environmental Remediation: Are We a Step Closer To Achieving Sustainability? Chem. Rev. 2016;116(12):7159-329.

Accepted MS

[203] Zhou C, Lai C, Xu P, Zeng G, Huang D, Li Z, et al. Rational Design of Carbon-Doped Carbon Nitride/$Bi_{12}O_{17}Cl_2$ Composites: A Promising Candidate Photocatalyst for Boosting Visible-Light-Driven Photocatalytic Degradation of Tetracycline. ACS Sustain. Chem. Eng. 2018;6(5):6941-6949.

[204] Yang Y, Zhang C, Huang D, Zeng G, Huang J, Lai C, et al. Boron nitride quantum dots decorated ultrathin porous g-$C_3N_4$: Intensified exciton dissociation and charge transfer for promoting visible-light-driven molecular oxygen activation. Appl. Catal. B: Environ. 2019;245:87-99.

[205] Zhang M, Zhang Y, Tang L, Zeng G, Wang J, Zhu Y, et al. Ultrathin Bi2WO6 nanosheets loaded g-$C_3N_4$ quantum dots: A direct Z-scheme photocatalyst with enhanced photocatalytic activity towards degradation of organic pollutants under wide spectrum light irradiation. J. Colloid Interface Sci. 2019;539:654-64.

[206] Jiang L, Yuan X, Zeng G, Chen X, Wu Z, Liang J, et al. Phosphorus- and Sulfur-Codoped g-$C_3N_4$: Facile Preparation, Mechanism Insight, and Application as Efficient Photocatalyst for Tetracycline and Methyl Orange Degradation under Visible Light Irradiation. ACS Sustain. Chem. Eng. 2017;5(7):5831-41.

[207] Zhou C, Xu P, Lai C, Zhang C, Zeng G, Huang D, et al. Rational design of graphic carbon nitride copolymers by molecular doping for visible-light-driven degradation of aqueous sulfamethazine and hydrogen evolution. Chem. Eng. J. 2019;359:186-96.

[208] Jiang L, Yuan X, Zeng G, Liang J, Wu Z, Wang H. Construction of an all-solid-state Z-scheme photocatalyst based on graphite carbon nitride and its

Accepted MS

enhancement to catalytic activity. Environ. Sci. Nano. 2018;5(3):599-615.

[209] Fu J, Chang B, Tian Y, Xi F, Dong X. Novel $C_3N_4$–CdS composite photocatalysts with organic–inorganic heterojunctions: in situ synthesis, exceptional activity, high stability and photocatalytic mechanism. J. Mater. Chem. A. 2013;1(9):3083.

[210] Yan SC, Li ZS, Zou ZG. Photodegradation of rhodamine B and methyl orange over boron-doped g-$C_3N_4$ under visible light irradiation. Langmuir : the ACS journal of surfaces and colloids. 2010;26(6):3894-901.

[211] Katsumata H, Sakai T, Suzuki T, Kaneco S. Highly Efficient Photocatalytic Activity of g-$C_3N_4$/$Ag_3PO_4$ Hybrid Photocatalysts through Z-Scheme Photocatalytic Mechanism under Visible Light. Ind. Eng. Chem. Res. 2014;53(19):8018-25.

[212] Chen D, Wu S, Fang J, Lu S, Zhou G, Feng W, et al. A nanosheet-like α-$Bi_2O_3$/g-$C_3N_4$ heterostructure modified by plasmonic metallic Bi and oxygen vacancies with high photodegradation activity of organic pollutants. Sep. Purif. Technol. 2018;193:232-41.

[213] Wang X, Wang H, Yu K, Hu X. Immobilization of 2D/2D structured g-$C_3N_4$ nanosheet/reduced graphene oxide hybrids on 3D nickel foam and its photocatalytic performance. Mater. Res. Bull. 2018;97:306-13.

[214] Guo H, Niu H-Y, Liang C, Niu C-G, Huang D-W, Zhang L, et al. Insight into the energy band alignment of magnetically separable $Ag_2O$/$ZnFe_2O_4$ p-n heterostructure with rapid charge transfer assisted visible light photocatalysis. J. Catal. 2019;370:289-303.

Accepted MS

[215] Guo H, Niu C-G, Huang D-W, Tang N, Liang C, Zhang L, et al. Integrating the plasmonic effect and p-n heterojunction into a novel $Ag/Ag_2O/PbBiO_2Br$ photocatalyst: Broadened light absorption and accelerated charge separation co-mediated highly efficient visible/NIR light photocatalysis. Chem. Eng. J. 2019;360:349-63.

[216] Xiao T, Tang Z, Yang Y, Tang L, Zhou Y, Zou Z. In situ construction of hierarchical $WO_3/g\text{-}C_3N_4$ composite hollow microspheres as a Z-scheme photocatalyst for the degradation of antibiotics. Appl. Catal. B: Environ. 2018;220:417-28.

[217] Wang K, Zhang G, Li J, Li Y, Wu X. 0D/2D Z-Scheme Heterojunctions of Bismuth Tantalate Quantum Dots/Ultrathin $g\text{-}C_3N_4$ Nanosheets for Highly Efficient Visible Light Photocatalytic Degradation of Antibiotics. ACS Appl. Mater. Interfaces 2017;9(50):43704-15.

[218] Cheng M, Zeng G, Huang D, Lai C, Liu Y, Zhang C, et al. High adsorption of methylene blue by salicylic acid-methanol modified steel converter slag and evaluation of its mechanism. J. Colloid Interface Sci. 2018;515:232-9.

[219] Jiang L, Yuan X, Zeng G, Liang J, Wu Z, Wang H, et al. A facile band alignment of polymeric carbon nitride isotype heterojunctions for enhanced photocatalytic tetracycline degradation. Environ. Sci. Nano. 2018;5(11):2604-17.

[220] Yu H, Huang B, Wang H, Yuan X, Jiang L, Wu Z, et al. Facile construction of novel direct solid-state Z-scheme AgI/BiOBr photocatalysts for highly effective removal of ciprofloxacin under visible light exposure: Mineralization efficiency and

Accepted MS

mechanisms. J. Colloid Interface Sci. 2018;522:82-94.

[221] Han Q, Chen N, Zhang J, Qu L. Graphene/graphitic carbon nitride hybrids for catalysis. Materials Horizons. 2017;4(5):832-50.

[222] Zhu J, Xiao P, Li H, Carabineiro SA. Graphitic carbon nitride: synthesis, properties, and applications in catalysis. ACS Appl. Mater. Interfaces 2014;6(19):16449-65.

[223] Li Y, Sun Y, Dong F, Ho WK. Enhancing the photocatalytic activity of bulk g-$C_3N_4$ by introducing mesoporous structure and hybridizing with graphene. J. Colloid Interface Sci. 2014;436:29-36.

[224] Ou M, Wan S, Zhong Q, Zhang S, Song Y, Guo L, et al. Hierarchical Z-scheme photocatalyst of g-$C_3N_4$@Ag/$BiVO_4$(040) with enhanced visible-light-induced photocatalytic oxidation performance. Appl. Catal. B: Environ. 2018;221:97-107.

[225] Wu X-f, Zhao Z-h, Sun Y, Li H, Zhang C-x, Wang Y-j, et al. Preparation and characterization of $Ag_2CrO_4$/few layer boron nitride hybrids for visible-light-driven photocatalysis. J. Nanopart. Res. 2017;19(6):193.

[226] Song Y, Xu H, Wang C, Chen J, Yan J, Xu Y, et al. Graphene-analogue boron nitride/$Ag_3PO_4$ composite for efficient visible-light-driven photocatalysis. RSC Adv. 2014;4(100):56853-62.

[227] Weng Q, Ide Y, Wang X, Wang X, Zhang C, Jiang X, et al. Design of BN porous sheets with richly exposed (002) plane edges and their application as $TiO_2$ visible light sensitizer. Nano Energy. 2015;16:19-27.

[228] Abdelhaleem A, Chu W. Photodegradation of 4-chlorophenoxyacetic acid under

Accepted MS

visible LED activated N-doped $TiO_2$ and the mechanism of stepwise rate increment of the reused catalyst. J. Hazard. Mater. 2017;338:491-501.

[229] Cordero-Garcia A, Turnes Palomino G, Hinojosa-Reyes L, Guzman-Mar JL, Maya-Tevino L, Hernandez-Ramirez A. Photocatalytic behaviour of $WO_3/TiO_2$-N for diclofenac degradation using simulated solar radiation as an activation source. Environ. Sci. Pollut. Res. Int. 2017;24(5):4613-24.

[230] Abdelhaleem A, Chu W, Liang X. Diphenamid degradation via sulfite activation under visible LED using Fe (III) impregnated N-doped $TiO_2$ photocatalyst. Appl. Catal. B: Environ. 2019;244:823-35.

[231] Jiang J-X, Zhang Q-Q, Li Y-H, Li L. Three-dimensional network graphene aerogel for enhancing adsorption and visible light photocatalysis of nitrogen-doped $TiO_2$. Mater. Lett. 2019;234:298-301.

[232] Feng Y, Lu H, Gu X, Qiu J, Jia M, Huang C, et al. ZIF-8 derived porous N-doped ZnO with enhanced visible light-driven photocatalytic activity. J. Phys. Chem. Solids 2017;102:110-114.

[233] Kumar S, Baruah A, Tonda S, Kumar B, Shanker V, Sreedhar B. Cost-effective and eco-friendly synthesis of novel and stable N-doped ZnO/g-$C_3N_4$ core-shell nanoplates with excellent visible-light responsive photocatalysis. Nanoscale. 2014;6(9):4830-42.

[234] Wang F, Chen P, Feng Y, Xie Z, Liu Y, Su Y, et al. Facile synthesis of N-doped carbon dots/g-$C_3N_4$ photocatalyst with enhanced visible-light photocatalytic activity for the degradation of indomethacin. Appl. Catal. B: Environ. 2017;207:103-13.

Accepted MS

[235] Zhang J, Yuan X, Jiang L, Wu Z, Chen X, Wang H, et al. Highly efficient photocatalysis toward tetracycline of nitrogen doped carbon quantum dots sensitized bismuth tungstate based on interfacial charge transfer. J. Colloid Interface Sci. 2018;511:296-306.

[236] Liu C, Zhu H, Zhu Y, Dong P, Hou H, Xu Q, et al. Ordered layered N-doped $KTiNbO_5$/g-$C_3N_4$ heterojunction with enhanced visible light photocatalytic activity. Appl. Catal. B: Environ. 2018;228:54-63.

[237] Peter CN, Anku WW, Sharma R, Joshi GM, Shukla SK, Govender PP. N-doped ZnO/graphene oxide: a photostable photocatalyst for improved mineralization and photodegradation of organic dye under visible light. Ionics. 2018;25(1):327-39.

[238] Chen M, Xu P, Zeng G, Yang C, Huang D, Zhang J. Bioremediation of soils contaminated with polycyclic aromatic hydrocarbons, petroleum, pesticides, chlorophenols and heavy metals by composting: Applications, microbes and future research needs. Biotechnol. Adv. 2015;33(6):745-55.

[239] Cheng M, Zeng G, Huang D, Lai C, Xu P, Zhang C, et al. Hydroxyl radicals based advanced oxidation processes (AOPs) for remediation of soils contaminated with organic compounds: A review. Chem. Eng. J. 2016;284:582-98.

[240] Liang J, Yang Z, Tang L, Zeng G, Yu M, Li X, et al. Changes in heavy metal mobility and availability from contaminated wetland soil remediated with combined biochar-compost. Chemosphere. 2017;181:281-8.

[241] Li X, Xu P, Chen M, Zeng G, Wang D, Chen F, et al. Application of silver phosphate-based photocatalysts: Barriers and solutions. Chem. Eng. J.

Accepted MS

2019;366:339-57.

[242] Li X, Wen J, Low J, Fang Y, Yu J. Design and fabrication of semiconductor photocatalyst for photocatalytic reduction of $CO_2$ to solar fuel. Science China Materials. 2014;57(1):70-100.

[243] Inoue T, Fujishima A, Konishi S, Honda K. Photoelectrocatalytic reduction of carbon dioxide in aqueous suspensions of semiconductor powders. Nature. 1979;277(5698):637-8.

[244] Ye S, Wang R, Wu M-Z, Yuan Y-P. A review on g-$C_3N_4$ for photocatalytic water splitting and $CO_2$ reduction. Appl. Surf. Sci. 2015;358:15-27.

[245] Chang X, Wang T, Gong J. $CO_2$ photo-reduction: insights into $CO_2$ activation and reaction on surfaces of photocatalysts. Energy Environ. Sci. 2016;9(7):2177-96.

[246] Hong J, Zhang W, Ren J, Xu R. Photocatalytic reduction of $CO_2$: a brief review on product analysis and systematic methods. Anal. Methods 2013;5(5):1086.

[247] Qin J, Wang S, Ren H, Hou Y, Wang X. Photocatalytic reduction of $CO_2$ by graphitic carbon nitride polymers derived from urea and barbituric acid. Appl. Catal. B: Environ. 2015;179:1-8.

[248] Wang S, Lin J, Wang X. Semiconductor-redox catalysis promoted by metal-organic frameworks for $CO_2$ reduction. Physical chemistry chemical physics : PCCP. 2014;16(28):14656-60.

[249] Mao J, Peng T, Zhang X, Li K, Ye L, Zan L. Effect of graphitic carbon nitride microstructures on the activity and selectivity of photocatalytic $CO_2$ reduction under visible light. Catal. Sci. Technol. 2013;3(5):1253.

Accepted MS

[250] Yu W, Xu D, Peng T. Enhanced photocatalytic activity of g-$C_3N_4$ for selective $CO_2$ reduction to $CH_3OH$ via facile coupling of ZnO: a direct Z-scheme mechanism. J. Mater. Chem. A. 2015;3(39):19936-47.

[251] Kuriki R, Sekizawa K, Ishitani O, Maeda K. Visible-light-driven $CO_2$ reduction with carbon nitride: enhancing the activity of ruthenium catalysts. Angewandte Chemie. 2015;54(8):2406-9.

[252] Yuan Y-P, Cao S-W, Liao Y-S, Yin L-S, Xue C. Red phosphor/g-$C_3N_4$ heterojunction with enhanced photocatalytic activities for solar fuels production. Appl. Catal. B: Environ. 2013;140-141:164-8.

[253] Golberg D, Bando Y, Huang Y, Terao T, Mitome M, Tang C, et al. Boron nitride nanotubes and nanosheets. ACS nano. 2010;4(6):2979-93.

[254] Akple MS, Low J, Qin Z, Wageh S, Al Ghamdi AA, Yu J, et al. Nitrogen-doped $TiO_2$ microsheets with enhanced visible light photocatalytic activity for $CO_2$ reduction. Chin. J. Catal. 2015;36(12):2127-34.

[255] Núñez J, de la Peña O'Shea VA, Jana P, Coronado JM, Serrano DP. Effect of copper on the performance of ZnO and $ZnO_{1-x}N_x$ oxides as $CO_2$ photoreduction catalysts. Catal. Today 2013;209:21-7.

[256] Chen P, Wang H, Liu H, Ni Z, Li J, Zhou Y, et al. Directional electron delivery and enhanced reactants activation enable efficient photocatalytic air purification on amorphous carbon nitride co-functionalized with O/La. Appl. Catal. B: Environ. 2019;242:19-30.

[257] Li J, Zhang Z, Cui W, Wang H, Cen W, Johnson G, et al. The Spatially Oriented

Accepted MS

Charge Flow and Photocatalysis Mechanism on Internal van der Waals Heterostructures Enhanced g-$C_3N_4$. ACS Catal. 2018;8(9):8376-85.

[258] Li J, Dong Xa, Sun Y, Jiang G, Chu Y, Lee SC, et al. Tailoring the rate-determining step in photocatalysis via localized excess electrons for efficient and safe air cleaning. Appl. Catal. B: Environ. 2018;239:187-95.

[259] Cui W, Li J, Sun Y, Wang H, Jiang G, Lee SC, et al. Enhancing ROS generation and suppressing toxic intermediate production in photocatalytic NO oxidation on O/Ba co-functionalized amorphous carbon nitride. Appl. Catal. B: Environ. 2018;237:938-46.

[260] Dong Xa, Li J, Xing Q, Zhou Y, Huang H, Dong F. The activation of reactants and intermediates promotes the selective photocatalytic NO conversion on electron-localized Sr-intercalated g-$C_3N_4$. Appl. Catal. B: Environ. 2018;232:69-76.

[261] Cui W, Li J, Dong F, Sun Y, Jiang G, Cen W, et al. Highly Efficient Performance and Conversion Pathway of Photocatalytic NO Oxidation on SrO-Clusters@Amorphous Carbon Nitride. Environ. Sci. Technol. 2017;51(18):10682-90.

[262] Kroke E, Schwarz M, Horath-Bordon E, Kroll P, Noll B, Norman AD. Tri-s-triazine derivatives. Part I. From trichloro-tri-s-triazine to graphitic $C_3N_4$ structuresPart II: Alkalicyamelurates M3[C6N7O3], M = Li, Na, K, Rb, Cs, manuscript in preparation. New J. Chem. 2002;26(5):508-12.

[263] Zhu B, Zhang J, Jiang C, Cheng B, Yu J. First principle investigation of halogen-doped monolayer g-$C_3N_4$ photocatalyst. Appl. Catal. B: Environ.

Accepted MS

2017;207:27-34.

[264] Zhu B, Zhang L, Cheng B, Yu J. First-principle calculation study of tri-s-triazine-based g-$C_3N_4$: A review. Appl. Catal. B: Environ. 2018;224:983-99.

[265] Xiong T, Wang H, Zhou Y, Sun Y, Cen W, Huang H, et al. KCl-mediated dual electronic channels in layered g-$C_3N_4$ for enhanced visible light photocatalytic NO removal. Nanoscale. 2018;10(17):8066-8074.

[266] Shao B, Liu Z, Zeng G, Wu Z, Liu Y, Cheng M, et al. Nitrogen-Doped Hollow Mesoporous Carbon Spheres Modified g-$C_3N_4$/$Bi_2O_3$ Direct Dual Semiconductor Photocatalytic System with Enhanced Antibiotics Degradation under Visible Light. ACS Sustain. Chem. Eng. 2018;6(12):16424-36.

[267] Cui J, Liang S, Wang X, Zhang J. First principle modeling of oxygen-doped monolayer graphitic carbon nitride. Mater. Chem. Phys. 2015;161:194-200.

[268] Sudhaik A, Raizada P, Shandilya P, Jeong D-Y, Lim J-H, Singh P. Review on fabrication of graphitic carbon nitride based efficient nanocomposites for photodegradation of aqueous phase organic pollutants. J. Ind. Eng. Chem. 2018;67:28-51.

[269] Lu L, Lv Z, Si Y, Liu M, Zhang S. Recent progress on band and surface engineering of graphitic carbon nitride for artificial photosynthesis. Appl. Surf. Sci. 2018;462:693-712.

[270] Zhang Y, Yun J, Wang K, Chen X, Yang Z, Zhang Z, et al. First-principle study of graphyne-like BN sheet: Electronic structure and optical properties. Comput. Mater. Sci. 2017;136:12-9.

Accepted MS

[271] Ding S, Mao D, Yang S, Wang F, Meng L, Han M, et al. Graphene-analogue h-BN coupled Bi-rich $Bi_4O_5Br_2$ layered microspheres for enhanced visible-light photocatalytic activity and mechanism insight. Appl. Catal. B: Environ. 2017;210:386-99.

[272] Li L, Yu X, Yang X, Fang Y, Zhang X, Xu X, et al. Porous BN with vacancy defects for selective removal of CO from $H_2$ feed gas in hydrogen fuel cells: a DFT study. J. Mater. Chem. A. 2016;4(40):15631-7.

[273] Zhou X, Chu W, Zhou Y, Sun W, Xue Y. DFT simulation on H2 adsorption over Ni-decorated defective h-BN nanosheets. Appl. Surf. Sci. 2018;439:246-53.

[274] Yu W, Zhang J, Peng T. New insight into the enhanced photocatalytic activity of N-, C- and S-doped ZnO photocatalysts. Appl. Catal. B: Environ. 2016;181:220-7.

[275] Zheng Z, Cox M, Li B. Surface modification of hexagonal boron nitride nanomaterials: a review. J. Mater. Sci. 2017;53(1):66-99.

[276] Pakdel A, Zhi C, Bando Y, Golberg D. Low-dimensional boron nitride nanomaterials. Mater. Today. 2012;15(6):256-65.

[277] Lee D, Lee B, Park KH, Ryu HJ, Jeon S, Hong SH. Scalable exfoliation process for highly soluble boron nitride nanoplatelets by hydroxide-assisted ball milling. Nano lett. 2015;15(2):1238-44.

[278] Zhang J, Hu S, Wang Y. A convenient method to prepare a novel alkali metal sodium doped carbon nitride photocatalyst with a tunable band structure. RSC Adv. 2014;4(108):62912-9.

[279] Liu D, Zhang M, Xie W, Sun L, Chen Y, Lei W. Porous BN/$TiO_2$ hybrid

Accepted MS

nanosheets as highly efficient visible-light-driven photocatalysts. Appl. Catal. B: Environ. 2017;207:72-8.

[280] Ji M, Xia J, Di J, Liu Y, Chen R, Chen Z, et al. Graphene-like boron nitride induced accelerated charge transfer for boosting the photocatalytic behavior of $Bi_4O_5I_2$ towards bisphenol a removal. Chem. Eng. J. 2018;331:355-63.

[281] Liu D, Cui W, Lin J, Xue Y, Huang Y, Li J, et al. A novel $TiO_{2-x}N_x$/BN composite photocatalyst: Synthesis, characterization and enhanced photocatalytic activity for Rhodamine B degradation under visible light. Catal. Commun. 2014;57:9-13.

[282] Li X, Qi F, Xue Y, Yu C, Jia H, Bai Y, et al. Porous boron nitride coupled with CdS for adsorption–photocatalytic synergistic removal of RhB. RSC Adv. 2016;6(101):99165-71.

[283] Wu X-F, Li H, Sun Y, Wang Y-J, Zhang C-X, Su J-Z, et al. Synthesis of $SnS_2$/few layer boron nitride nanosheets composites as a novel material for visible-light-driven photocatalysis. Appl. Phys. A. 2017;123(11).

[284] Doong R-a, Liao C-Y. Enhanced photocatalytic activity of Cu-deposited N-$TiO_2$/titanate nanotubes under UV and visible light irradiations. Sep. Purif. Technol. 2017;179:403-11.

[285] Sun S, Sun M, Kong Y, Liu F, Yu Z, Anandan S, et al. One-step thermal synthesis of Ag-modified g-$C_3N_4$/N-doped $TiO_2$ hybrids with enhanced visible-light photocatalytic activity. J. Mater. Sci. 2016;52(2):1183-93.

[286] Lu N, Shao C, Li X, Miao F, Wang K, Liu Y. A facile fabrication of

Accepted MS

nitrogen-doped electrospun $In_2O_3$ nanofibers with improved visible-light photocatalytic activity. Appl. Surf. Sci. 2017;391:668-76.

[287] Lv W, He J, Xu A, Hu L, Da L. Structure and Photocatalytic Activity of Nitrogen-doped $HTiNbO_5$ Nanosheet Aggregation. Nano. 2017;12(01):1750003.

Accepted MS

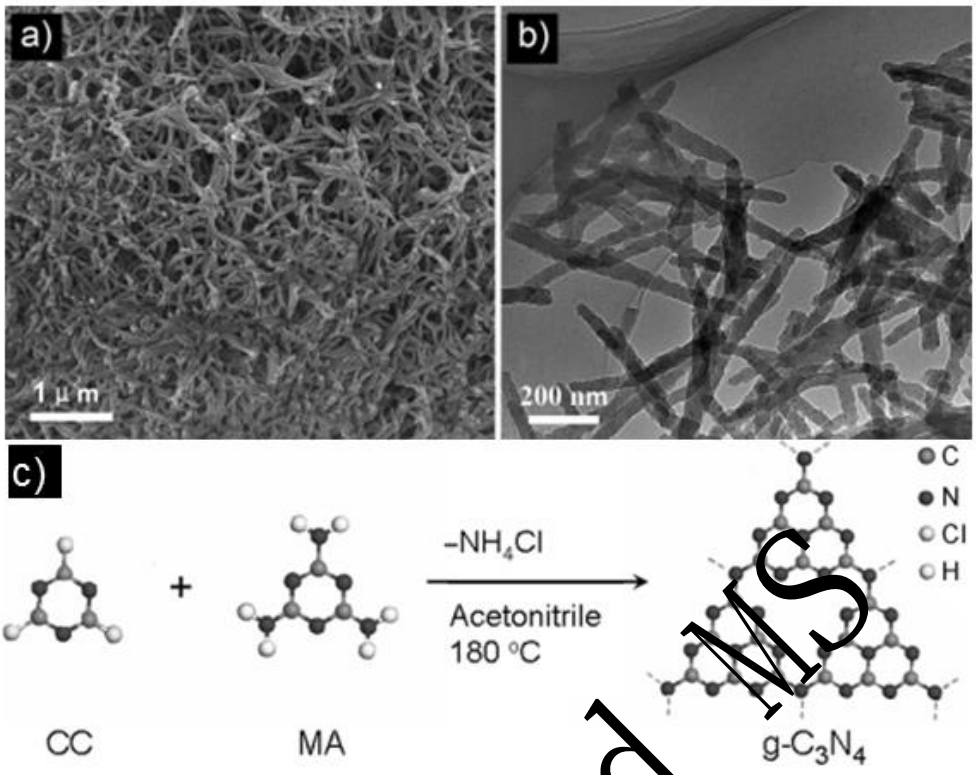


Fig.1. (a) SEM and (b) TEM images of g-$C_3N_4$ nanorod networks; (c) polymerization processes of cyanuric chloride (CC) and melamine (MA) in subcritical acetonitrile solvent. Reprinted with permission from ref. [80] Copyright 2012 Wiley.

Accepted MS

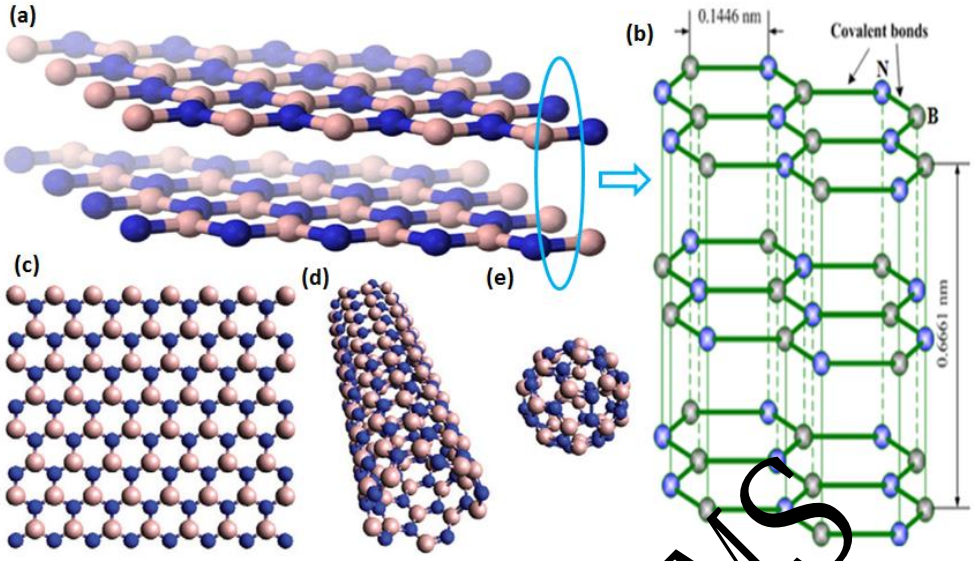


Fig.2. (a-b) Structural models and corresponding parameters of h-BN layer; (c-e) Structural models of 2D, 1D and 0D h-BN nanostructures. (a) is reprinted with permission from ref. [275] Copyright 2017 Springer. (b) is reprinted with permission from ref. [95] Copyright 2015 American Chemical Society. (c, d and e) is reprinted with permission from ref. [276] Copyright 2012 Elsevier.

Accepted MS

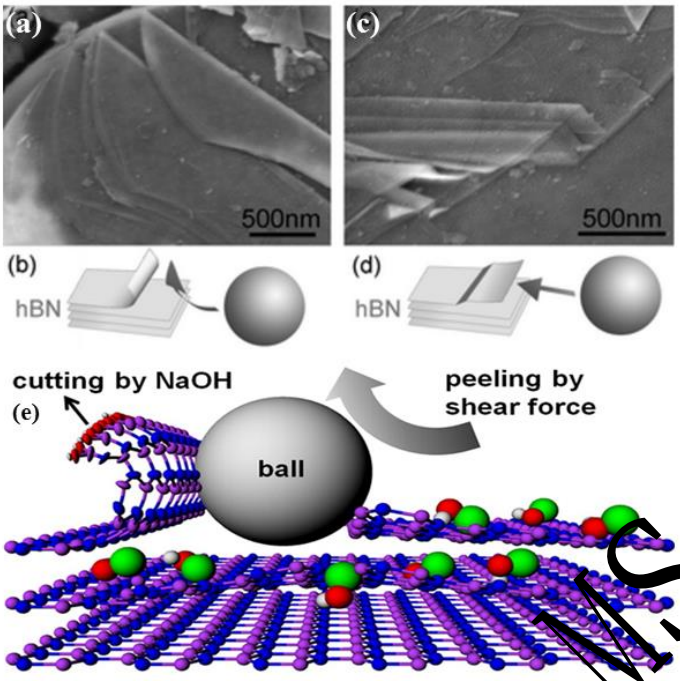


Fig.3 (a and c) SEM images of BN nanosheets and (b, d and e) Exfoliation mechanisms and model of wet ball milling method. (a-d) are reprinted with permission from ref. [99] Copyright 2011 Royal Society of Chemistry. (e) is reprinted with permission from ref. [277] Copyright 2015 American Chemical Society.

Accepted MS

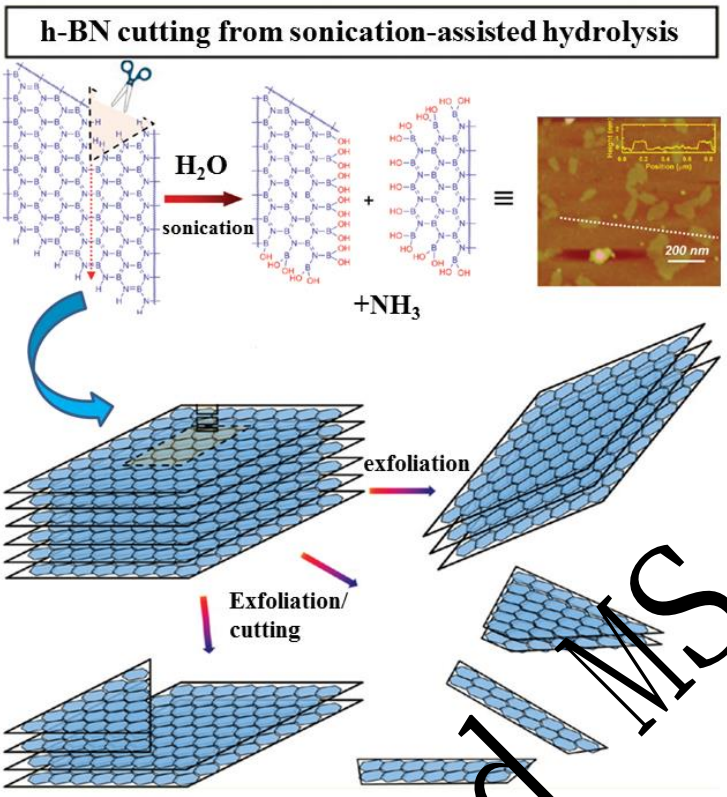


Fig.4 Sonication—assisted hydrolysis and exfoliation mechanism of h-BN. Reprinted with permission from ref. [114] Copyright 2011 American Chemical Society.

Accepted MS

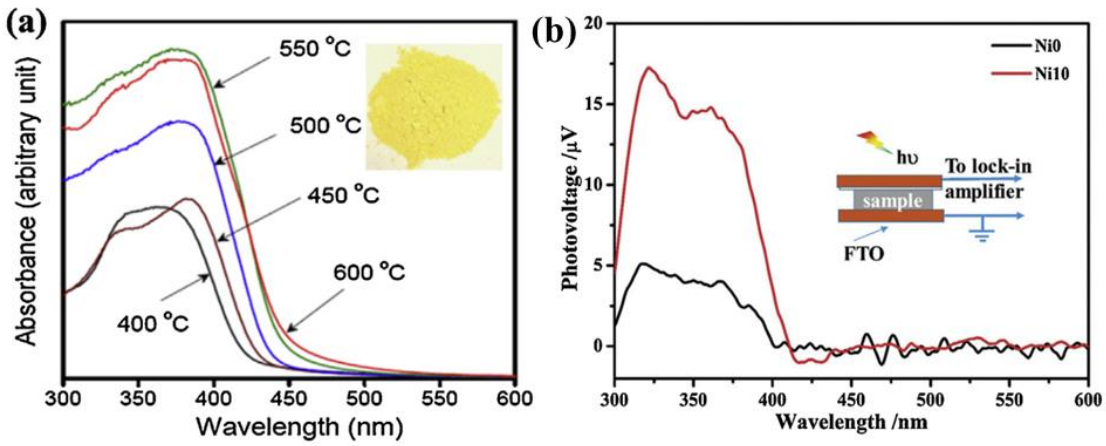


Fig.5 (a) UV/Vis absorption spectra of g-$C_3N_4$ prepared at different temperature. Inset: photograph of the photocatalyst [126] Copyright 2017 Elsevier; (b) SPV of g-$C_3N_4$ (Ni0) and Ni@g-$C_3N_4$ (Ni10). The inset shows the schematic setup of SPV measurements [138] Copyright 2015 Royal Society of Chemistry.

Accepted MS

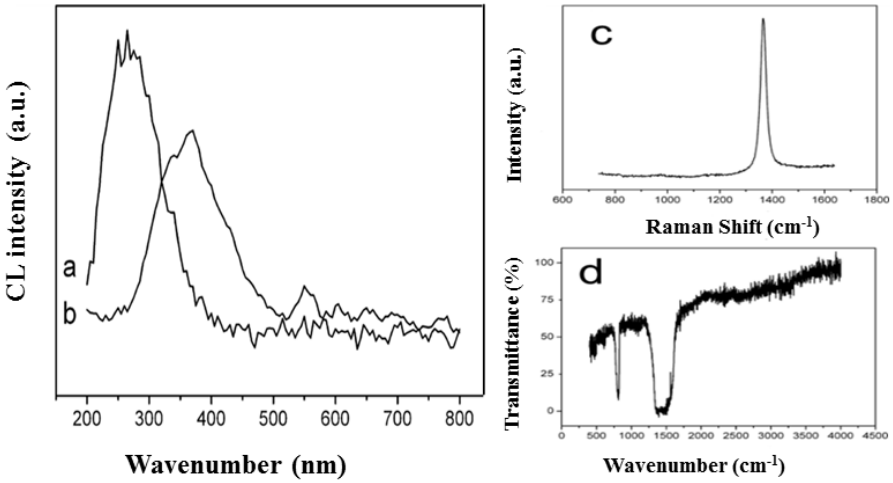


Fig.6 Typical CL spectra of the BNNSs (a) and granular films (b); Typical Raman (c) and FTIR (d) spectra of the BNNSs. Reprinted with permission from ref. [145] Copyright 2010 American Chemical Society.

Accepted MS

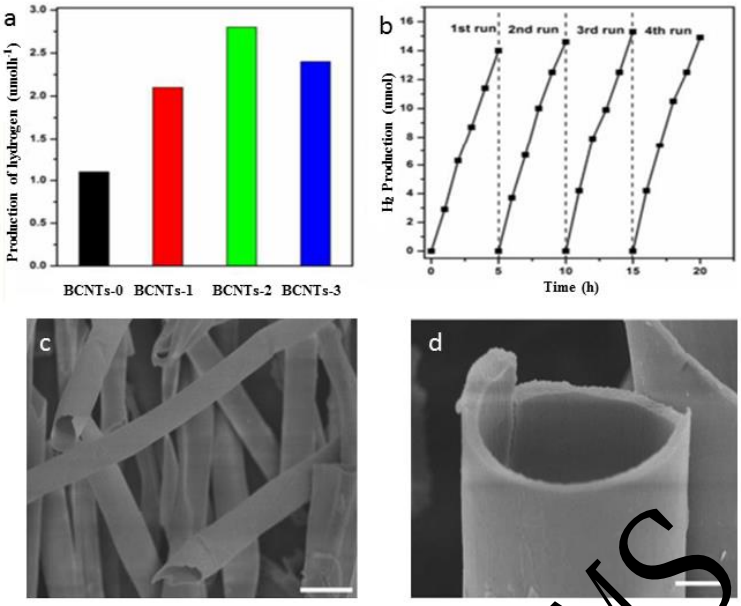


Fig.7 (a) Photocatalytic water splitting activity of 1.0wt% Pt-loaded BCNTs samples under visible light (λ>420 nm) illumination. (b) Cyclic stability test of hydrogen evolution by 1.0wt% Pt-loaded BCNTs-2 under visible light illumination for 20h. (c, d) SEM images of BCNTs-2 sample, scale bar, 50 μm and 5 μm, respectively. Reprinted with permission from ref. [178] Copyright 2017 Royal Society of Chemistry.

Accepted MS

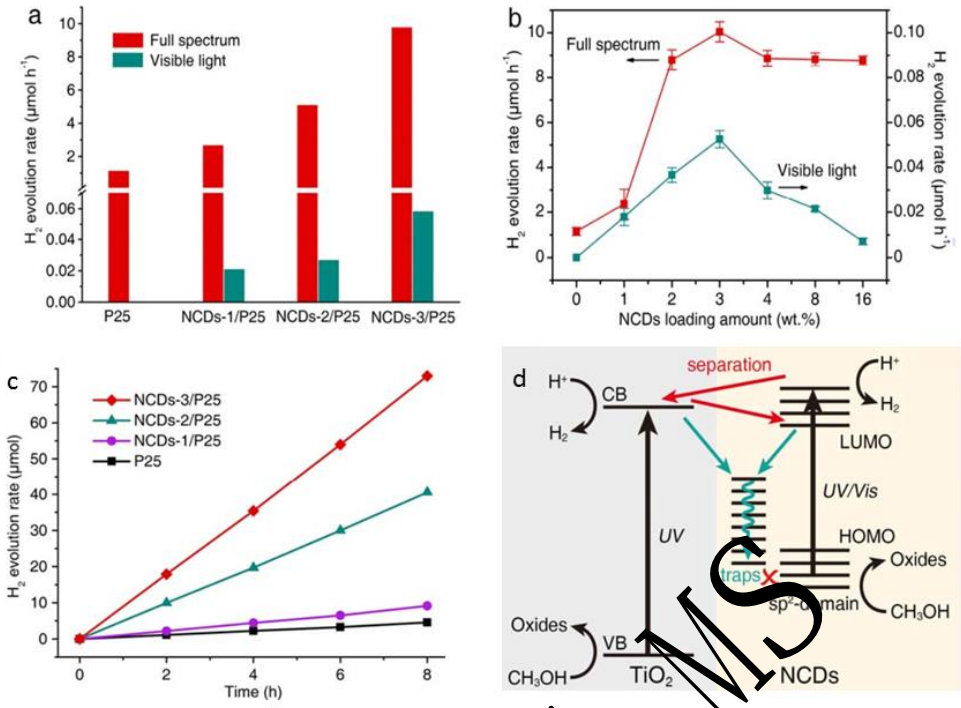


Fig.8 Photocatalytic $H_2$ evolution rates in 25 vol.% methanol (a) for pure P25 $TiO_2$ and NCDs/P25 composites and (b) for NCDs-3/P25 composites with different NCDs loadings under full spectrum and visible light (λ >450 nm) illumination. (c) Photocatalytic stability tests under full spectrum illumination. (d) Schematic illustration of the electron transfer mechanisms. Reprinted with permission from ref [182]. Copyright 2017 Wiley.

Accepted MS

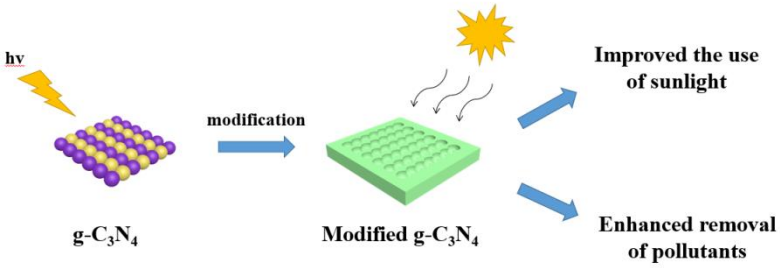


Fig.9 The advantages of modified g-$C_3N_4$ with minor modifications from ref [58]. Copyright 2015 Elsevier.

Accepted MS

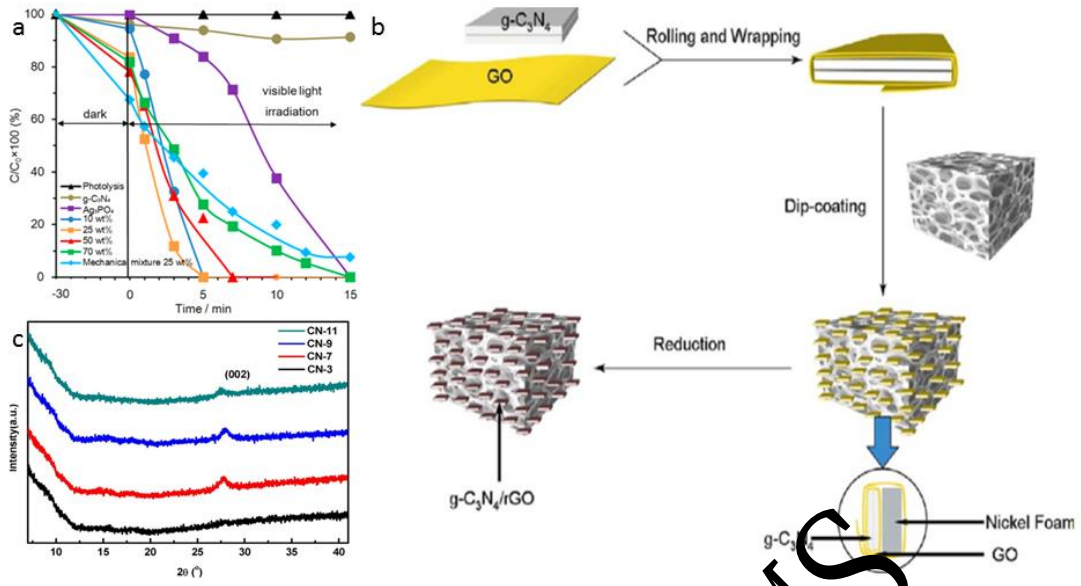


Fig.10 (a) Photocatalytic activities of g-$C_3N_4$, $Ag_3PO_4$ and 10, 25, 50, and 70 wt% g-$C_3N_4$/$Ag_3PO_4$ hybrid photocatalysts on the decolorization of MO under visible-light irradiation (>440 nm). (b) Proposed formation mechanism of g-$C_3N_4$/rGO coatings immobilized on nickel foam. (c) Partial enlarged XRD patterns of as-prepared g-$C_3N_4$/rGO hybrid coatings immobilized on nickel foam. (a) is reprinted with permission from ref [211]. Copyright 2014 American Chemical Society; (b-c) are reprinted with permission from ref [213]. Copyright 2018 Elsevier.

Accepted MS

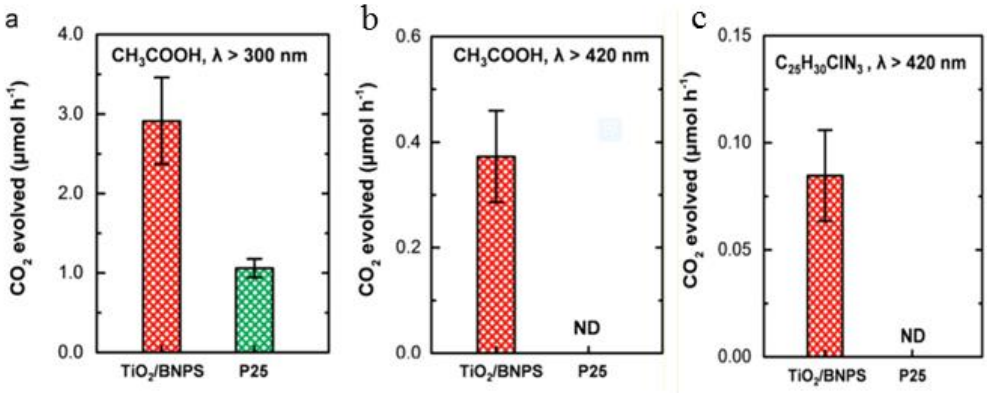


Fig.11 $CO_2$ evolved rates of acetic acid photocatalytic oxidations by $TiO_2$/BNPS composite with the comparison to commercial P25 ($TiO_2$) under λ>300 nm irradiation (a), and under λ>420 nm irradiation conditions (b). (c) $CO_2$ evolved rates of crystal violet photocatalytic oxidations by the composite under the λ>420 nm irradiation. Reprinted with permission from ref [227]. Copyright 2015 Elsevier.

Accepted MS

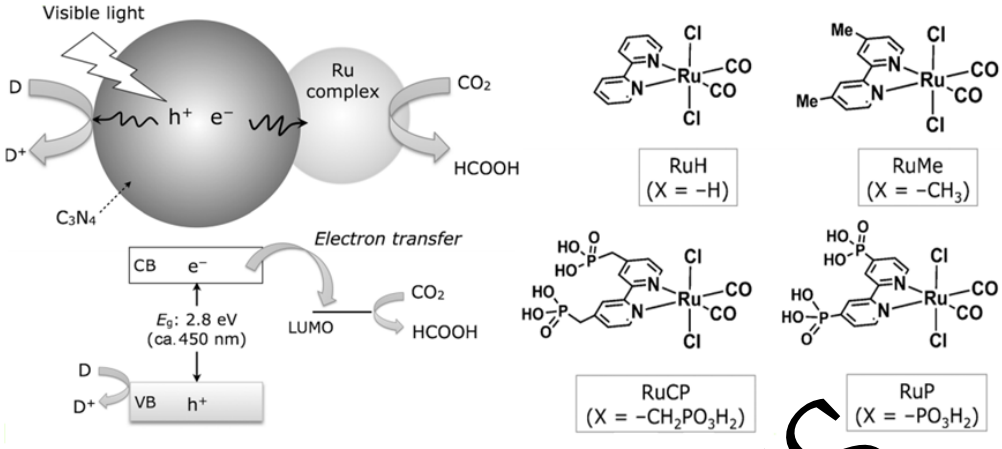


Fig.12 $CO_2$ reduction using a Ru complex/$C_3N_4$ hybrid photocatalyst, along with structures of the Ru complexes used. CB=conduction band, VB=valence band. Reprinted with permission from ref [251] Copyright 2015 Wiley.

Accepted MS

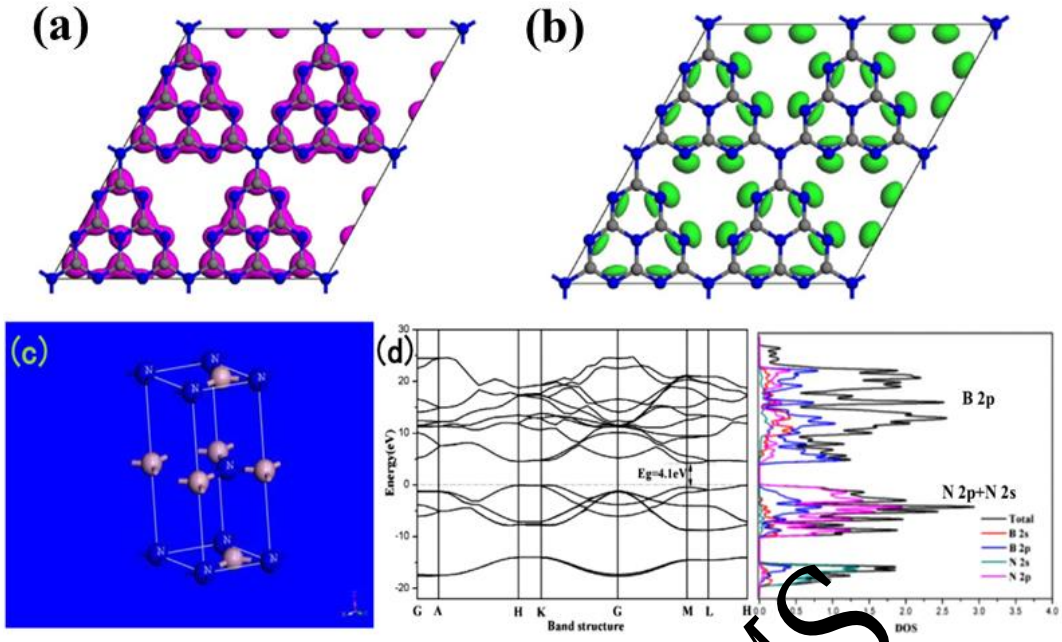


Fig.13 Calculated LUMO (a) and HOMO (b) of monolayer g-$C_3N_4$. Reprinted with permission from ref [263]. Copyright 2017 Elsevier. Crystal structures, calculated band structures and density of states of (c, d) h-BN. Reprinted with permission from ref [271]. Copyright 2017 Elsevier.

Accepted MS

Table 1 Summary of methods synthesized g-$C_3N_4$ and BN.

| Photocatalysts | Methods | Advantages | Disadvantages | Morphology | Ref |
|---|---|---|---|---|---|
| g-$C_3N_4$ | Solvothermal method | cheap raw materials; uniformity of the reaction system; less pollution; mild reaction conditions; | difficulty to controlled the reaction conditions and realized industrial production | 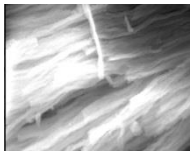 | [80-82] |
| | Solid-state reaction | control the morphology of g-$C_3N_4$ | reaction conditions is difficult | 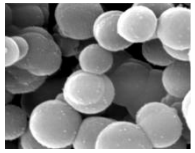 | [83, 84] |
| | Thermal polymerization | simple experimental operation; Short preparation cycle; large productivity | the product is not pure; generate harmful gas | 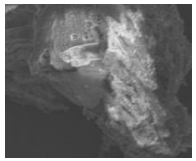 | [93, 94] |
| | Electrochemistry deposition | simple equipment; easy control; no high temperature and high pressure | energy pollution | 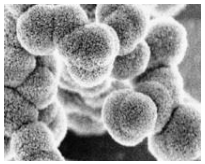 | [87-89] |

Accepted MS

| | | | | | |
|---|---|---|---|---|---|
| BN | Mechanical exfoliation | perfectly crystalline structures; high quality BN nanosheets; | yield is very low; hard to control; difficult to produce on a large scale. | 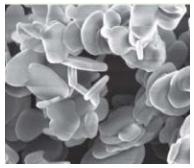 | [98-100] |
| | chemical vapor deposition | simple and easy to control; high yield; perfectly crystalline structures; | high cost; process immaturity | 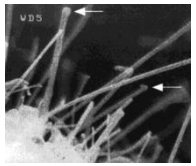 | [101-103] |
| | chemical exfoliation | high quality BN nanosheets; easy to control; | yield is not high; environment pollution; | 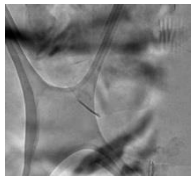 | [112, 113] |
| | liquid-phase exfoliation | large quantities; high quality; | hard to control the number of layers and the lateral size | 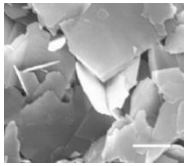 | [114] |

Accepted MS

Table 2 crystal structure parameters of boron nitride.

| **Type** | **Crystalline forms** | **Crystalline structure** | **Hybrid methods** | **Crystal structures** |
|---|---|---|---|---|
| h-BN | hexagonal | layer structure | $sp^2$ | 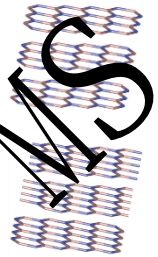 |
| r-BN | rhombohedral | layer structure | $sp^2$ | |
| c-BN | cubic | blende | $sp^3$ | 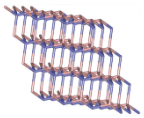 |
| w-BN | wurtzite | wurtzite | $sp^3$ | 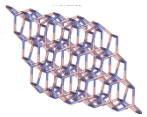 |

Accepted MS

Table 3. g-$C_3N_4$ based and their properties.

| Composite type | Precursor | Photocatalytic activity | Light source | Main active species | Ref (year) |
|---|---|---|---|---|---|
| CdS/g-$C_3N_4$ | $Cd(NO_3)_2 \cdot 4H_2O$ and thiourea (CdS) | Degradation of MO and 4-ABA | 300 W Xe lamp with a 420 nm cutoff filter | $h^+$ and $\bullet O_2^-$ | [209] |
| | melamine (CN) | k=0.123 $min^{-1}$ and 73% degradation after 1h , respectively | | | (2013) |
| Bi/α-$Bi_2O_3$/g-$C_3N_4$ | $Bi(NO_3)_3 \cdot 5H_2O$ (α-$Bi_2O_3$) | Degradation of Tetracycline and RhB | 300 W Xe lamp with a 400 nm cutoff filter | $h^+$ and $\bullet O_2^-$ | [212] |
| | urea (CN) | 90.2% and 95.6% degradation after 180 min and 90 min , respectively | | | (2018) |
| Cl/g-$C_3N_4$ | ammonium chloride (Cl) | Degradation of NO and RhB | 150 W Xe lamp with a 400 nm cutoff filter | $h^+$ and $\bullet OH$ | [47] |
| | melamine (CN) | about 60% degradation after 2.5h and k=0.9 $h^{-1}$ , respectively | | | (2017) |
| B/g-$C_3N_4$ | boron oxide (B) | Degradation of MO and RhB | 300 W Xe lamp with a 420 nm cutoff filter | $h^+$ and $\bullet O_2^-$ | [210] |
| | melamine (CN) | k=0.061 $min^{-1}$ and k=0.199 $min^{-1}$ , respectively | | | (2010) |
| $Ag_3PO_4$/g-$C_3N_4$ | $AgNO_3$ and $Na_3PO_4$($Ag_3PO_4$) | Degradation of MO | 300 W Xe lamp with a 420 nm cutoff filter | $h^+$ and $\bullet O_2^-$ | [211] |
| | urea (CN) | almost 100% degradation only 5 minute | | | (2014) |
| rGO/g-$C_3N_4$ | urea and dicyandiamide (CN) | Degradation of MO and TC | 300 W Xe lamp with a 400 nm cutoff filter | $h^+$ and $\bullet O_2^-$ | [213] |

Accepted MS

| | | | | | |
|---|---|---|---|---|---|
| | | 97% degradation after 3h and 90% degradation after 2h , respectively | | | (2018) |
| $WO_3/g\text{-}C_3N_4$ | $Na_2WO_4$ ($WO_3$) | Degradation of Ceftiofur sodium | 300 W Xe lamp with a 420 nm cutoff filter | $h^+$ and •OH | [216] |
| | dicyandiamide (CN) | 82% degradation after 2h | | | (2018) |
| $Bi_3TaO_7$ QDs/$g\text{-}C_3N_4$ | $Bi(NO_3)_3$ $5H_2O$ and $TaCl_5$ ($Bi_3TaO_7$) | Degradation of CIP | 300 W Xe lamp with a 420 nm cutoff filter | •OH and $•O_2^-$ | [217] |
| | dicyandiamide (CN) | 91% degradation after 2h | | | (2017) |
| $Ag/BiVO_4/g\text{-}C_3N_4$ | $Bi(NO_3)_3$ $5H_2O$ and $AgNO_3$ ($Ag/BiVO_4$) | Degradation of NO | 350 W Xe lamp with a 420 nm cutoff filter | •OH and $•O_2^-$ | [224] |
| | melamine (CN) | 83% degradation after 2.5h | | | (2017) |
| Na/ $g\text{-}C_3N_4$ | NaOH (Na) | Degradation of RhB | 300 W Xe lamp with a 420 nm cutoff filter | •OH and $•O_2^-$ | [278] |
| | dicyandiamide (CN) | k=0.0001 $min^{-1}$ | | | (2014) |
| K/ $g\text{-}C_3N_4$ | KOH (K) | Degradation of RhB | 300 W Xe lamp with a 420 nm cutoff filter | •OH and $•O_2^-$ | [48] |
| | dicyandiamide (CN) | k=0.011 $min^{-1}$ | | | (2015) |

Accepted MS

Table 4. BN based and their properties.

| Composite type | Precursor | Photocatalytic activity | Light source | Main active species | Ref (year) |
|---|---|---|---|---|---|
| $Ag_2CrO_4$/BN | $K_2CrO_4$ and $AgNO_3$ | Degradation of RhB | 300 W Xe lamp with a 420 nm cutoff filte | $h^+$ and $\bullet O_2^-$ | [225] |
| | hexagonal BN | k=0.027 $min^{-1}$ and 97% degradation after 2h , respectively | | | (2017) |
| $Ag_3PO_4$/BN | $AgNO_3$ and $Na_3PO_4$ | Degradation of RhB | 300 W Xe lamp with a 400 nm cutoff filte | $h^+$ and $\bullet O_2^-$ | [226] |
| | hexagonal BN | k=0.28 $min^{-1}$ and 97% degradation after 2h , respectively | | | (2014) |
| BN/$TiO_2$ | guanidine hydrochloride | Degradation of RhB and phenol | 300 W Xe lamp with a 420 nm and 300 nm cutoff filte, respectively | $h^+$ and $\bullet O_2^-$ | [279] |
| | boron trioxide and $TiO_2$ | 99% degradation after 6 h | | | (2017) |
| BN/$Bi_4O_5I_2$ | $Bi(NO_3)_3$ $5H_2O$ and BN | Degradation of bisphenol A and RhB | 300 W Xe lamp with a 400 nm cutoff filte | $h^+$ and $\bullet O_2^-$ | [280] |
| | 1-hexyl-3-methylimidazolium iodide | 91% degradation after 20 min | | | (2018) |
| $TiO_{2-x}N_x$/BN | tetrabutyl titanate | Degradation of RhB | 250 W halide lamp with a 400 nm cutoff filte | $h^+$ and $\bullet O_2^-$ | [281] |
| | melamine–boron acid adducts | 97.8% degradation after 40 min | | | (2014) |
| CdS/BN | boric acid and melamine | Degradation of RhB | 300 W Xe lamp with a 420 nm cutoff filte | $h^+$ and $\bullet O_2^-$ | [282] |

Accepted MS

| | | | | | |
|---|---|---|---|---|---|
| | CdS | 74% degradation after 80 min | | | (2016) |
| $SnS_2$/BN | $SnCl_4$ $5H_2O$ and thioacetamide | Degradation of RhB | 300 W Xe lamp with a 420 nm cutoff filte | •OH | [283] |
| | hexagonal BN | 93.7% degradation after 210 min | | | (2017) |
| BN/g-$C_3N_4$ | melamine and BN | Degradation of RhB and TC | 300 W Xe lamp with a 420 nm cutoff filte | $h^+$ and •$O_2^-$ | [46] |
| | | 99.5% degradation after 40 min and 79.7% degradation after 1h , respectively | | | (2018) |

Accepted MS

Table 5. N-doped and their properties.

| Composite type | Precursor | Photocatalytic activity | Light source | Main active species | Ref (year) |
|---|---|---|---|---|---|
| Cu deposited N-$TiO_2$/ | standard $TiO_2$ | Degradation of bisphenol A (BPA) | Four 8 W UV or visible lamps with a 420 nm cutoff filte | $h^+$ and •OH | [284] |
| titanate nanotubes | $NH_3/N_2$ atmosphere | k=0.012 $min^{-1}$ and 93% degradation after 240 min | | | (2017) |
| Ag-modified g-$C_3N_4$/ | melamine and TiN | Degradation of methyl blue (MB) | 500 W Xe lamp with a 420 nm cutoff filte | •$O_2^-$ and •OH | [285] |
| N-doped $TiO_2$ | $AgNO_3$ | k=0.0201 $min^{-1}$ and about 80% degradation after 80 min | | | (2017) |
| N-$TiO_2$ | urea | Degradation of 4-chlorophenoxyacetic acid (4-CPA) | two visible white LED lamps of 100 W | $h^+$ and •OH | [228] |
| | titanium isopropoxide | 95% degradation after 240 min | | | (2017) |
| N-doped ZnO | zinc nitrate hexahydrate | Degradation of RhB | 300 W Xe lamp with a 420 nm cutoff filte | no data | [232] |
| | ammonium hydroxide solution | about 80% degradation after 180 min | | | (2017) |
| $WO_3/TiO_2$-N | tetrabutyl orthotitanate | Degradation of diclofenac | 1500 W Xe lamp with a 420 nm cutoff filte | •$O_2^-$ and •OH | [229] |
| | ammonium (para) tungstate hydrate | about 92% degradation after 120 min | | | (2016) |
| N-$In_2O_3$ | $In(NO_3)_3 \cdot 4.5H_2O$ and $NH_3$ | Degradation of RhB | 150 W Xe lamp with a 420 nm cutoff filte | no data | [286] |

Accepted MS

| | | | | | |
|---|---|---|---|---|---|
| | | 97% degradation after 180 min | | | (2016) |
| N-doped ZnO/ | zinc nitrate and melamine | Degradation of RhB | 300 W Xe lamp with a 400 nm cutoff filte | $O_2^{\bullet -}$ and $\bullet OH$ | [233] |
| g-$C_3N_4$ | ammonium oxalate | k=0.0679 $min^{-1}$ and about 98% degradation after 60 min | | | (2014) |
| N-doped carbon dots/ | citric acid and urea | Degradation of indomethacin (IDM) | 350 W Xe lamp with a 420 nm cutoff filte | $h^+$ and $\bullet O_2^{\bullet -}$ | [234] |
| g-$C_3N_4$ | dicyandiamide | k=0.0272 $min^{-1}$ and about 91.5% degradation after 90 min | | | (2017) |
| N-HTiNbO$_5$ | $K_2CO_3$, $Nb_2O_5$ and $TiO_2$ | Degradation of methylene blue (MB) | 500 W Xe lamp with a 420 nm cutoff filte | no data | [287] |
| | ammonia atmosphere | about 54% degradation after 170 min | | | (2017) |
| N-CQDs/$Bi_2WO_6$ | ammonium citrate | Degradation of TC | 300 W Xe lamp with a 420 nm cutoff filte | $h^+$ and $\bullet O_2^-$ | [235] |
| | $Bi(NO_3)_3$ $5H_2O$ and $Na_2WO_4$ $2H_2O$ | about 97% degradation after 25 min | | | (2018) |
| N-KTiNbO$_5$/ | $K_2CO_3$, $Nb_2O_5$ and $TiO_2$ | Degradation of RhB | 300 W Xe lamp with a 420 nm cutoff filte | $h^+$ and $\bullet O_2^-$ | [236] |
| g-$C_3N_4$ | melamine | about 100% degradation after 80 min | | | (2018) |
| N-ZnO/GO | zinc acetate dihydrate and urea | Degradation of brilliant smart green (BG) | 300 W Xe lamp with a 420 nm cutoff filte | $\bullet O_2^-$ | [237] |
| | graphite flakes | about 99% degradation after 90 min | | | (2018) |

Accepted MS

Table 6: The main products of $CO_2$ and corresponding reduction potential with reference to NHE at pH of 7.

| **Product** | **Reaction** | **$E^0$** |
|---|---|---|
| Hydrogen | $2H_2O + 2e^- \longrightarrow 2OH^- + H_2$ | -0.41 |
| Methane | $CO_2 + 8H^+ + 8\,e^- \longrightarrow CH_4 + 2H_2O$ | -0.24 |
| Carbon monoxide | $CO_2 + 2H+ + 2\,e^- \longrightarrow CO + H_2O$ | -0.51 |
| Methanol | $CO_2 + 6H+ + 6\,e^- \longrightarrow CH_3OH + H_2O$ | -0.39 |
| Formic acid | $CO_2 + 2H^+ + 2e^- \longrightarrow HCOOH$ | -0.58 |
| Ethane | $2CO_2 + 14H^+ + 14e^- \longrightarrow C_2H_6 + 4H_2O$ | -0.27 |
| Ethanol | $2CO_2 + 12H^+ + 12e^- \longrightarrow C_2H_5OH + 3H_2O$ | -0.33 |
| Oxalate | $2CO2 + 2H^+ + 2e^- \longrightarrow H_2C_2O_4$ | -0.87 |

Accepted MS